CRANFIELD UNIVERSITY

A SANSICA

ACTIVE DEBRIS REMOVAL MISSION FROM LEO WITH ELECTRIC AND HYBRID PROPULSION

SCHOOL OF ENGINEERING
Department of Aerospace Engineering

MASTER BY RESEARCH THESIS
Academic year: 2010-11

Supervisor: S. Hobbs
December 2011

CRANFIELD UNIVERSITY

SCHOOL OF ENGINEERING
Department of Aerospace Engineering

MASTER BY RESEARCH THESIS

Academic year: 2010-11

A SANSICA

Active debris removal mission from LEO with electric and hybrid propulsion

Supervisor: S Hobbs

December 2011

The thesis is submitted in partial fulfilment of the requirements for the degree of Master of Science

Contents

List of Figures

List of Tables

List of Symbols

β Yaw Thrust Angle

ΔV Velocity Variation (Impulsive)

$\dot{\Omega}$ Precession Rate

$\dot{m}$ Flow Mass Rate

μ Earth's Gravitational Constant

Ω Right Ascension of the Ascending Node

Ω_{in} Initial Right Ascension of the Ascending Node

ρ Density

Θ True Anomaly

ξ Specific Energy of the Spacecraft

A_D Debris Drag Area

C_D Drag Coefficient

f_{drag} Specific Drag

I_{sp} Specific Impulse

J_2 Earth's Gravity Term

m_{del} Delivered Mass by the Launcher

m_D Dry Mass of the Debris

m_d Dry Mass

m_{fin} Final Mass of the Spacecraft

m_{in} Initial Mass of the Spacecraft

$m_{p,J2}$ Propellant Mass for Drag Cancellation

$m_{p,podo}$ Propellant Mass for Transfer between Parking Orbit to Debris Orbit

$m_{p,re}$ Propellant Mass for Re-entry

$m_{p,tot}$ Total Propellant Mass for the Mission

m_p Propellant Mass

m_r Retrieved Mass by the Robotic Arm

N_D Number of Debris

R_E Earth's Radius

t_{podo} Duration of the Transfer between Parking Orbit and Debris Orbit

t_{re} Duration of Re-entry Manoeuvre

t_{tot} Total Duration of the Mission

t_{trans} Transfer duration

$t_{w,po}$ Waiting Time on Parking Orbit

u_{eq} Exhaust Velocity

$V_{A,HTO}$ Apogee Velocity in Hohmann Transfer Orbit

$V_{circ,do}$ Circular Velocity in Debris Orbit

A Drag Area

a Semi-major Axis

ADR Active Debris Removal mission

AS Analytical Approximated Solution

ASAT Anti-Satellite

D Drag

do Debris Orbit

DR LEO Debris Removal mission from LEO

E Eccentric Anomaly

e Eccentricity

EA Edelbaum Algorithm

FEEP Field Emission Electric Propulsion

g Standard Gravity Acceleration

GEO Geosynchronous Earth Orbit

h Height

HP High Performance

i Inclination

IADC International Debris Coordination Committee

ISO International Organization for Standard

LEO Low Earth Orbit

LP Low Performance

MM Mass Margin

NM Numerical Model

p Semi-latus Rectum

PCU Power Control Unit

PFS Propellant Feeding System

po Parking Orbit

PPT Pulsed Plasma Thruster

r Distance from Earth's centre

RAAN Right Ascension of the Ascending Node

RPR Relative Precession Rate

SPT Stationary Plasma Thruster

T Thrust

t Time

TDK Thruster De-orbiting Kit

V Velocity

Chapter 1

Introduction

Debris proliferation in space environment is an impending problem for preserving future missions. Although prevention measures (IADC guidelines, NASA Handbook for Limiting Orbit Debris) with the intent to regulate and limit the space trac are adopted, the necessity to reduce the increasing quantity of space debris leads to the will to conceive and test the effectiveness of active debris removal missions (ADR). ADR missions are devised for controlling the number of large objects, such as launch vehicle orbital stages or derelict spacecraft which no longer serve a useful purpose [1], orbiting in densely populated and commercially interesting areas (Sun-Synchronous Orbit, SSO).

1.1 Aims and Objectives

The aim of this study is to offer a credible and effective solution for an active space debris removal mission, proposing itself as a benchmark against which other mission proposal could be compared. By providing a preliminary analysis to choose the most efficient propulsion system, it is necessary to reduce the specific cost of de-orbited mass and collision risk in orbit.

As well as mitigation guidelines and traffic management provided by IADC normative, good solution for control space debris proliferation are active removal missions. Unlike anti-satellite activities (ASAT technologies), active debris removal missions (ADR) are conceived with the final aim to de-orbit launcher upper-stages and satellites at the end of their operative lives.

A future prospective for controlling space debris proliferation in LEO is presented in figure 1.1, where the effective number of objects with dimensions greater than 10 cm will be regulated by ADR missions starting in 2020, and will remove 5, 10 and 20 debris per year [2].

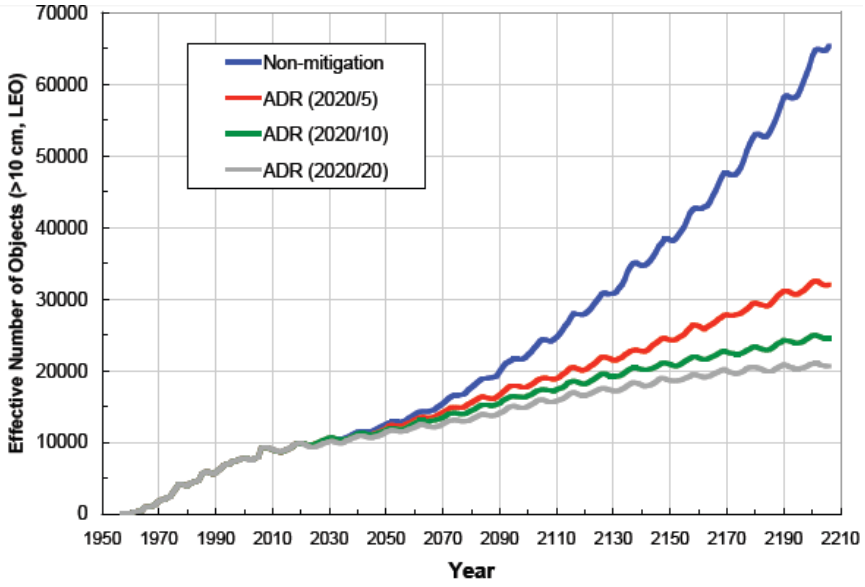

Figura 1.1: Potential benefits of ADR missions [2]

The European Space Agency keeps a database which catalogues orbiting debris, assigning them reference numbers and sorting them by orbital characteristics and status.

Target selection concerns Ariane IV upper stages, which has now been decommisioned and substituted with Ariane V. The presence of these upper stages represents a priority for the European space community in terms of debris proliferation control in LEO. These targets have a high mass and are in a densely populated orbit region. To reduce the probability of a collision in orbit, it is necessary to remove as much debris as possible. The mission architecture should also be suitable for other target typologies.

The main concept of this mission is to provide, after a rendezvous between spacecraft and target, grapple and dock with the target to be de-orbited.

The Ariane IV upper stage is represented as a cylinder with a circular cross section area and has the following size:

Ariane IV Upper Stage	
Mass (kg)	1600
Lenght (m)	11
Diameter (m)	2.7

Table 1.1: Target definition

The targets are on circular orbits and their characteristics in terms of name, reference number by ESA catalogue, height, inclination and right ascension of the ascending node are listed in table 1.2.

Name	Ref. N.	Height (km)	Inclin. (deg)	$\Omega_{in,do}$(deg)
ARIANE 40 R/B	20443	772.77	98.6278	135.0506
ARIANE 40 R/B	21610	763.15	98.6849	148.2152
ARIANE 40 R/B	22830	791.95	98.6247	124.3251
ARIANE 40+ R/B	23561	772.23	98.4873	124.1231
ARIANE 40+3 R/B	23608	610.45	98.2389	304.3863
ARIANE 40 R/B	25261	787.42	98.2256	167.2464
ARIANE 40 R/B	25979	617.80	98.1337	260.9017
ARIANE 40 DEB	35955	789.97	98.6001	124.4851

Table 1.2: Target debris orbit parameters [7]

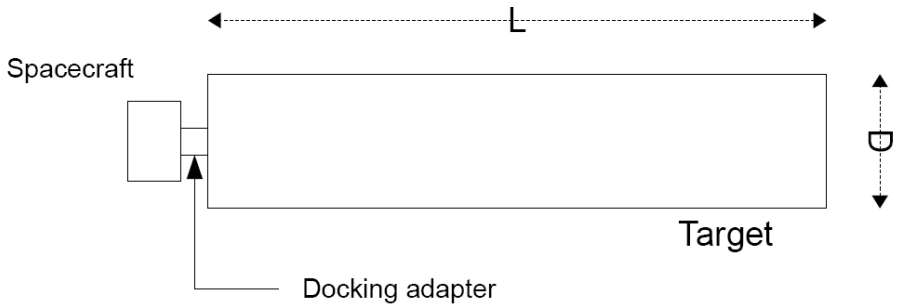

Figure 1.2: Simple model for the docked target

1.2 Organization of Report

After an introduction to the problem studied, explaining which the most important topics are and what the proposal for solving the problem is, the mission

simulation is illustrated. The code architecture and numerical methods are described for all the propulsion systems presented.

Assumptions and manoeuvres analysis are conducted for each proposal; chemical, electric and hybrid (chemical and electric combined) propulsion systems. The results are reported for each system and comparisons between the different solutions are discussed, emphasising on issues such as key assumptions or architecture options and selection. In the conclusion, further developments for the project are proposed.

Also, an appendix about the model for spacecraft mass estimation is presented.

Chapter 2

Literature Review

The main topics related to the study are presented for explaining why they are significant for the project and how they are connected to the solution proposed.

2.1 Space Debris

Space debris is one of the most pertinent problems in the space environment, in terms of achievement in the success of the mission. The increasing risk of collision with active spacecraft and the danger for astronauts during extra-vehicular operations highlights the necessity to catalogue space objects defined as debris and to create a normative for their disposal.

NASA defines space debris as "artificial objects, including derelict spacecraft and spent launch vehicle orbital stages, left in orbit which no longer serve a useful purpose" [1]. Abandoned spacecrafts, upper stages, objects related to human missions and fragments generated by previous explosions are part of this definition.

In both low-Earth orbits (LEO) and on geosynchronous Earth orbit (GEO), space debris proliferation has grown exponentially in recent decades and, currently, it is possible to count 20,000 objects with dimension greater than 10 cm, 500,000 with dimension between 1 and 10 cm and around 10 millions of particles with dimension smaller than 1 cm [1].

2.2 Mitigation Procedures

During the disposal mission of the SPOT-1 satellite, a heliosynchronous satellite used for Earth observation, the French space Agency (CNES) redacted a document approved by the IADC (International Debris Coordination Committee) proposing standard procedures with the aim to reduce space debris proliferation [3]. French mitigation guidelines limit the orbital lifetime to 25 years and the disposal manoeuvres consist of three steps:

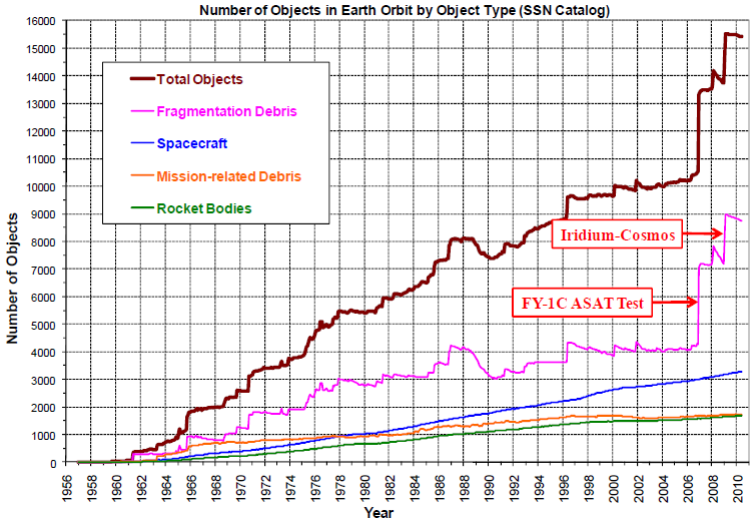

Figure 2.1: Number of objects catalogued by U.S. Space Surveillance Network (SSN) [8]

- Move the satellite from its operational orbit, avoiding collisions with other satellites of the same family
- De-orbit the satellite in atmosphere lowering the perigee with apogee boosts.
- Empty the tanks, battery and telemetry emitter disconnection.

Another important procedure is passivation [4]. To avoid future explosions, the residual propellant mass at the end of the mission is passivated. In zero gravity conditions it is difficult to precisely estimate this quantity, introducing uncertainties on the reliability of the disposal process.

Other operations also introduce uncertainties on the reliability of the disposal process. The International Organization for Standard (ISO) translated the IADC normative in engineering guidelines, requesting a reliability of 90% for disposal operations of spacecraft.

The American policy about preservation of space missions is expressed in a handbook of requirements and standards for space debris disposal operations. For debris in GEO the "NASA Handbook for Limiting Orbital Debris" [5] requires that after the disposal procedure, debris has to be 200 km above GEO for at least 100 years. Concerning the debris in LEO, operative lifetime is limited to 25 years after the completion of the mission and never more than 30 years from the launch, where upon they have to be de-orbited in atmosphere. Risks for human beings following the re-entry of the target are estimated by tables which include input data as kinetic energy and height of the operative orbit.

This study has the aim of proposing realistic and effective solutions for controlling space debris proliferation in LEO, by conceiving active debris removal mission for minimising the specific cost of de-orbited mass and collision risk for operative and orbiting spacecraft.

2.3 Active Debris Removal

Along with mitigation measures proposed by international organisations, active debris removal missions are the most effective method to control space debris proliferation.

DR LEO mission design provides a conventional technology baseline for removing ve Ariane IV upper stages in Sun-Synchronous orbits near 700 km altitude, since they have high mass and occupy a densely-populated orbit region.

The baseline concept of the DR LEO mission is to use a stack of similar spacecraft launched together and placed in the same parking orbit[1], characterised by a specific height and inclination. In turn.Each spacecraft in turn performs a rendez-vous with its target and de-orbit it in atmosphere, in a South Pacific area to minimize the risk to damage terrestrial properties and persons (figure 2.2).

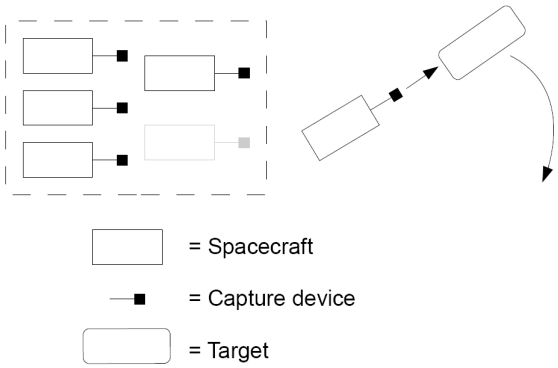

Figure 2.2: Schematization of the baseline concept for DR LEO mission

Different mission architectures can be conceived and proposed for controlling the number of objects in the space environment. Other ADR mission are proposed for removing five targets per year, with a final aim of de-orbiting 35 targets in seven years [6].

At this state of art, it is important to verify the effectivness and feasibility of active debris removal, regardless the specific mission architecture, presenting these preliminary projects as a baseline for further developments.

[1]Parking orbits always are considered to be circular

2.4 Mission Design

By quantifying the total mass, in terms of dry mass of the spacecraft and propellant mass, for removing 5-10 large debris items per year and knowing the delivered mass in parking orbit by the launcher it is possible to estimate the number of debris removable with a single launch or mission. Thus, the mass margin is defined as the delivered mass in the parking orbit by the launcher (m_{del}) minus the necessary mass for target re-entry, sum of dry mass of the spacecraft (m_d) and the propellant mass needed for all the orbital manoeuvres ($m_{p,tot}$).

With N_D number of debris/target, the mass margin is defined as follow:

$$MM = m_{del} - \sum_{i=1}^{N_D} (m_d^i + m_{p,tot}^i) \tag{2.1}$$

The $m_{p,tot}^i$ term is the total propellant mass related to the disposal of the $i-th$ target and is sum of propellant mass to perform the α–th manoeuvre:

$$m_{p,tot}^i = \sum_{\alpha} m_{p,\alpha}^i \tag{2.2}$$

Launcher and spacecraft characteristics, which are represented as delivered mass in parking orbit and dry mass respectively, are discussed in the following sections.

The mission has the peculiarity to consider as perturbative effects the atmospheric drag and gravitational term J2, due to the Earth's oblateness, during all the manoeuvres.

Reduction of the specific cost of delivered mass is translated in the maximisation of the mass margin. A high mass margin leads to the possibility to take on board more spacecraft, or, equivalently, remove more debris with a single launch or mission.

2.4.1 Manoeuvres Definition

For each target, the disposal mission is characterised by the following manoeuvres:

- Atmospheric drag cancellation in the parking orbit
- Transfer from parking orbit to target orbit
- Re-entry

Due to the J2 effect, parking and target orbit plans precede in a different way, because of the dependence on height and inclination. By using this relative precession rate, it is possible to align the lines of nodes, avoiding to perform an expansive manoeuvre in terms of propellant mass. Since these two orbits have a different initial right ascension of the ascending node (Ω_{in}), it is necessary to

wait for the alignment. During the alignment, the spacecraft is in the parking orbit and it needs to compensate the atmospheric drag that causes the height lowering.

For a circular orbit, the precession rate is:

$$\frac{d\Omega}{dt} = -\frac{3}{2}\frac{J_2 \cdot R_E^2}{r^2} \cdot \sqrt{\frac{\mu}{r}} \cdot \cos i \tag{2.3}$$

where R_E is the Earth's radius and μ the Earth's gravitational constant [9].

After the atmospheric drag cancellation, rendezvous between the spacecraft/chaser and the debris is performed. The transfer occurs to increase the height and for the plane change, in a combined manoeuvre. Respect with the selected propulsion system, the manoeuvres are impulsive or have a continuous low-thrust and are described by different set of equations.

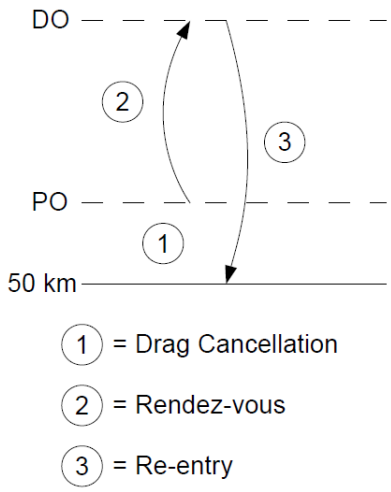

Figure 2.3: Mission architecture

Once the rendezvous is performed and after grappling and docking operations by means of a robotic arm takes place, the target is de-orbited in atmosphere. The re-entry procedure is different depending on the propulsion system used. The mission architecture is represented schematically in figure 2.3.

It is important to underline that atmospheric drag effects during the rendezvous is a further obstacle. In the re-entry this creates benefits as the velocity reduction of the spacecraft leads to propellant mass being saved.

The main challange of the study is to find the most efficient system between chemical and electric propulsion. Whilst with chemical engines impulsive manoeuvres are treated, electric propulsion systems use a continuous low thrust. Mainly used for controlling the spacecraft attitude in orbit, in this preliminary project electric engines are adopted for rendezvous and re-entry manoeuvres.

2.4.2 Launch Vehicle Selection

It would be desiderable to programme one mission using European technologies, more specifically the Russian launch vehicle Soyuz 2-1b. This vehicle satisfies the requirements for the allocation of the stack of spacecraft and the upper stage, Fregat, has the capability of de-orbiting itself which avoids creating new space debris.

	Soyuz 2-1b
Capability (tonne)	4
Cost (M$)	30 - 50
Nb of S/C	5
Cost/Target (M$)	12 - 15

Table 2.1: Launch vehicle selection - Soyuz 2-1b [11]

Launcher performance, in terms of delivered mass in the parking orbit, is estimated by linearly interpolating the data in table 2.2. This represents the mass delivered if the launch is from the base in Kourou to elio-synchronous and polar orbits.

	Elio-Synchronus		Polar	
h (km)	i (deg)	Mass (kg)	i (deg)	Mass (kg)
400	97.03	5270	90	5030
500	97.40	5146	90	5015
600	97.78	5010	90	5000
700	98.18	4880	90	4975
800	98.60	4760	90	4945
900	99.03	4630	90	4915
1000	99.48	4510	90	4880
1100	99.94	4392	90	4843
1200	100.42	4275	90	4805
1300	100.91	4160	90	4765
1400	101.42	4045	90	4720
1500	101.95	3935	90	4680
1600	102.50	3820	90	4640

Table 2.2: Launcher performance [12]

2.4.3 Spacecraft Definition

It is important to understand how the propulsion system influences the propellant mass necessary for orbital manoeuvres. The propulsion systems considered are:

- chemical

- electric
- hybrid (chemical and electric)

Hybrid propulsion is not carried out in the conventional way, with solid fuel and liquid oxidant, but is the combination of both chemical and electric propulsion engines or systems. Whilst the hybrid system is described in appendix A, the characteristics of chemical and electric propulsion systems are:

System	$m_d(kg)$	$I_{sp}(s)$	C_D	$A(m^2)$
Chemical	389.5	312	2.2	4
Electric	382.3	1640	2.2	4

Table 2.3: Propulsion systems parameters

The most significant parameters used in the code are listed as follows: dry mass, specific impulse, atmospheric drag coefficient and drag cross section. These values have been chosen carefully following estimations about the required power and mass of subsystems. The mass and power budgets found in 'DR LEO: Summary of the Group Design Project' by Dr. Stephen Hobbs [13] are presented in tables 2.4 and 2.5 below.

Propulsion System	Chemical	Electric
Sub-System	Mass (kg)	Mass (kg)
Structure	100	100
Engine	50.9	29
Tank	25.4	1.3
AOCS	29.3	29.3
OBDH	25	25
Communication	3	3
Thermal	20	20
Power	31.1	70.3
Payload	69	69
Mechanisms	17.2	17.2
TOT (+5% Margin)	389.5	382.3

Tabella 2.4: Mass budget

Propulsion System	Chemical		Electric	
Sub-System	Average (W)	Peak (W)	Average (W)	Peak (W)
AOCS	21.8	70.6	21.8	70.6
OBDH	35	35	35	35
Communication	3	3	3	3
Thermal	40	75	40	75
Power	12	29	39	100
Payload	139	295	139	295
TOT	250.8	507.6	277.8	578.6

Tabella 2.5: Power budget

In the chemical propulsion system, the engine that has been selected is the commercially used S400-12 by Astrium. This is characterized by a specific impulse and thrust that are equal to $I_{sp} = 312\,s$ and $T = 420\,N$ respectively. This engine uses a classic bi-propellant with MMH (MonoMethylHydrazine) and N2O4 (dinitrogen tetroxide or nitrogen peroxide) [13].

For the electric propulsion system, the engine consists of Hall thrusters fuelled with xenon as Snecma PPS-1350-G, by ESA with $I_{sp} = 1640\,s$ and $T = 68\,mN$ [13] respectively.

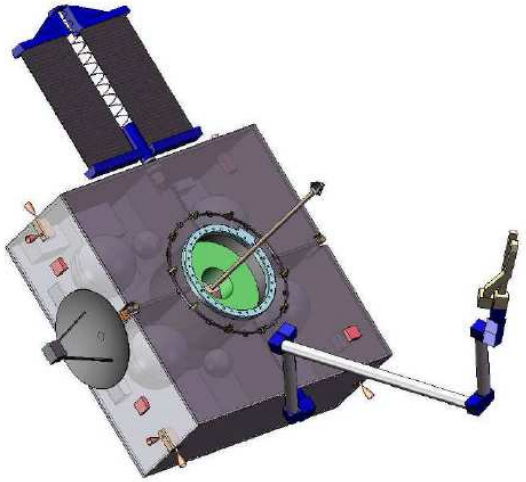

Figura 2.4: Standard Spacecraft Chaser [13]

2.5 Electric Propulsion

The predisposition in using rockets from military ballistic missiles for the development of commercial purposes was forced by the competition between USA

and USSR during the Cold War. The competition was rife until it was overtaken by the Space Race, which prompted the desire of flying into space.

By performing vertical launches from the ground and orbital manoeuvres during space missions require propellant mass to be stored in the spacecraft. The propellant mass consumption needs to be taken into great consideration during the design phase.

For historical and technological reasons, chemical propulsion is the conventional system installed in a vehicle used for space purposes. With a thrust-weight ratio between 10 and 30, this is the most affordable and safer propulsion system for vertical launch. For space manoeuvres other propulsion systems are used but chemical propulsion reduces the duration of the mission with a high reliability.

Due to the high mass ratio and low specific impulse, and consequently a high propellant consumption, other propulsion systems are proposed. Electric propulsion is one interesting and achievable system for space missions. This is characterised by a high specific impulse and is used for north-south station keeping manoeuvres because of its low performance in terms of thrust.

The main classification is based on the force required to accelerate the spacecraft:

- Thermo-gasdynamics: Resistojet and arcjet
- Electro-static: Field Emission Electric Propulsion (FEEP), Ion, Hall
- Effect Electro-magnetic: Pulsed Plasma Thruster (PPT)

The propulsion systems used in this report will be discussed successively.

Chapter 3

Mission Simulation

In this chapter the attention is focused on the description of a methodology based on the utilisation of scientific software and codes, with an emphasis on solving differential equations with numerical integration methods.

Convergence and stepsize control criteria used to ensure the quality of the solution are shown.

The intent is to develop a straightforward, reliable and effective code for different active debris removal scenarios, considering the most significant perturbation effects for the mission architecture conceived. This code needs to be able to analyse strategies for debris proliferation control in a space environment.

3.1 Code Documentation

The following view about code architecture gives an idea concerning the information and equations the user has to know and handle for solving the studied problem. With the aim to obtain the mass margin (MM) and relative precession rate (RPR) as a function of height and inclination of the parking orbit, the analysis is carried out for chemical and electric propulsion and subsequently, in the dedicated chapter, for hybrid systems.

The code requires the following subsystem parameters as input data:

- Launcher: delivered mass as a function of altitude and inclination of the parking orbit $m_{del} = f(r_{po}, i_{po})$
- Target / Debris: altitude r_{do}, inclination i_{do}, initial right ascension of the ascending node $RAAN_{in,do}$, mass of the target m_D, drag area of the target A_D, number of targets N_D.
- Spacecraft: dry mass m_d, specific impulse I_{sp}, drag area of the spacecraft $A_{s/c}$, drag coefficient C_D, initial right ascension of the ascending node $RAAN_{in,po}$, acceleration thrust for electric propulsion system a_T.

- Environment: Earth's gravitational constant μ, Earth's radius R_e, Earth's gravity term J_2, standard gravity g, atmospheric density as a function of the altitude $\rho(r)$.

The considered manoeuvres are:

- Drag Cancellation
- Non-coplanar transfer between parking orbit and target orbit
- Re-entry

The equation are differentiated for impulsive manoeuvres (chemical propulsion) and continuous low-thrust manoeuvres (electric propulsion):

- Impulsive: ΔV for impulsive manoeuvres, rocket's equation for propellant mass estimation, relative precession rate for line of nodes alignment, Lagrange's planetary equations for introduction of drag effects during transfers (iterative process).
- Continuous low-thrust: Runge-Kutta numerical methods for the integration of Lagrange's planetary equations in continuous low-thrust manoeuvres and drag effect, flow mass ratio definition for propellant mass estimation, relative precession rate for line of nodes alignment.

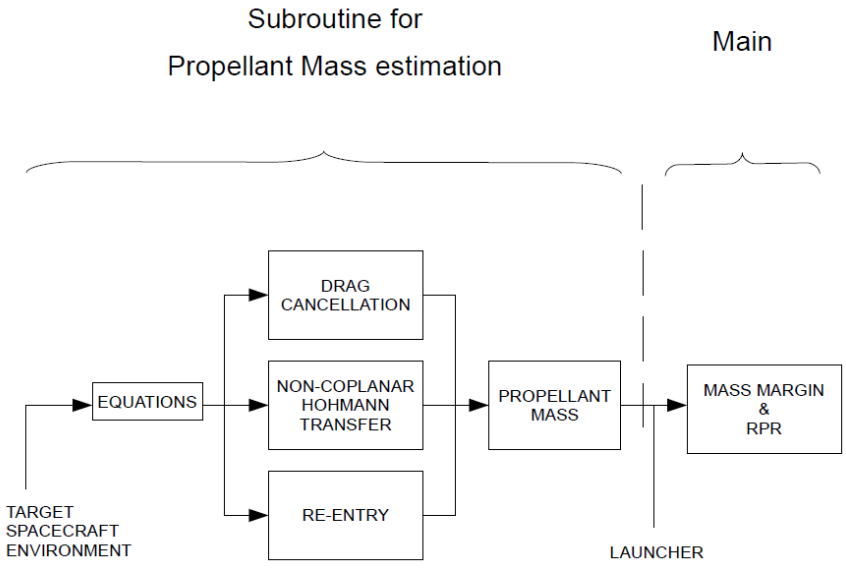

Figure 3.1: Code documentation

3.2 Numerical Methods

ODEs (Ordinary Differential Equations) can always be reduced to a set of N coupled first-order equations y_i [10].

With i = 0, ..., N-1 :

$$\frac{dy_i(x)}{dx} = f_i(x,\, y_0,\, ...,\, y_{N-1}) \tag{3.1}$$

where $i = 0,\, ...,\, N-1$ and f_i are known functions.

The choice of the method for solving the problem is the first decision to make. Obviously, depending on the boundary condition one method is preferred to another. The main categories of boundary conditions are:

- Initial conditions: where initial information is required to carry out the calculation.
- Two-point boundary conditions: information about the function in more than one point is required.

In this study, only the initial boundary condition is considered and all the first-order equations, obtained by the reduction of the ODEs, are re-written in finite steps Δy and Δx. Thus, it is possible to describe the variation of y when x varies with a Δx stepsize.

The numerical method analysed is Runge-Kutta, and more precisely first order Runge-Kutta or 'Euler Method', second order Runge-Kutta or 'Midpoint Method' and fourth order Runge-Kutta.

3.2.1 Runge-Kutta Method

The generic differential equation is:

$$\frac{dy}{dx} = f\,(x,\, y) \tag{3.2}$$

With a stepsize $\Delta x = h$, the studied methods are:

- Euler method:

$$y_{n+1} = y_n + h \cdot f\,(x_n,\, y_n) + o(h^2) \tag{3.3}$$

The step's error is $o(h^2)$; therefore the method is first order accurate.

- Midpoint method:

$$\begin{gathered} k_1 = h \cdot f\,(x_n,\, y_n) \\ k_2 = h \cdot f\,(x_n + \tfrac{h}{2},\, y_n + \tfrac{k_1}{2}) \\ y_{n+1} = y_n + k_2 + o(h^3) \end{gathered} \tag{3.4}$$

The step's error is $o(h^3)$; therefore the method is second order accurate.

- Fourth order Runge-Kutta

$$\begin{aligned} k_1 &= h \cdot f\left(x_n,\, y_n\right) \\ k_2 &= h \cdot f\left(x_n + \tfrac{h}{2},\, y_n + \tfrac{k_1}{2}\right) \\ k_3 &= h \cdot f\left(x_n + \tfrac{h}{2},\, y_n + \tfrac{k_2}{2}\right) \\ k_4 &= h \cdot f\left(x_n + h,\, y_n + k_3\right) \\ y_{n+1} &= y_n + \tfrac{1}{6}k_1 + \tfrac{1}{3}k_2 + \tfrac{1}{3}k_3 + \tfrac{1}{6}k_4 + o(h^5) \end{aligned} \tag{3.5}$$

The step's error is $o(h^5)$; therefore the method is fourth order accurate.

It is possible to continue to give other estimations of the right hand side of eq. (3.2), but for simplicity the analysis stops here.

3.2.2 Adaptive Stepsize Control for Runge-Kutta methods

To minimize the computational cost, it is interesting to understand where it is necessary to reduce or increase the stepsize during the numerical integration [10]. In this regard, by estimating the truncation error ϵ, defined as difference between two solution y_1 and y_2 respectively with two steps h and one step $2h$, and by fixing an error tolerance $\bar{\epsilon}$, if:

$$\epsilon =: \; |y_2 - y_1| \geq \bar{\epsilon} \tag{3.6}$$

is not acceptable and the integration has to be repeated with a smaller stepsize.

On other hand, '*err*', the truncation error over error tolerance ratio is defined as:

$$err = \frac{\epsilon}{\bar{\epsilon}} \leq 1 \tag{3.7}$$

For a generic Runge-Kutta method of the $N - th$ order, the truncation error scales as h^N. The function err behaves in the same way, and using this information it is possible to control the stepsize. If a step h_1 is related to an error err_1 and a step h_0 to err_0, the step h_0 can be obtained as follows:

$$h_0 = h_1 \left| \frac{err_0}{err_1} \right|^{1/N} \tag{3.8}$$

Depending on the err_0 over err_1 ratio, the equation (3.8) is used to understand if it is necessary to decrease or increase the stepsize.

3.2.3 Structure of the Sub-Routine

A schematic description of the routine for the numerical integration presents three levels: algorithm, stepsize controller and user interface [10].

The algorithm is the internal level and has to estimate the variation of the solution with a stepsize Δx. The stepsize controller, using the criteria described

in the previous section, chooses the integration step to guarantee the accuracy desired. The user interface starts and ends the integration, dialoguing with the user in terms of data storage and visualization.

3.3 Manoeuvres Architecture

The following flowcharts describe the code architectures schematically. The analysis is conducted for chemical and electric propulsion systems, whilst code documentation for hybrid system is delegated to the dedicated chapter.

3.3.1 Manoeuvres for Chemical Propulsion System

- Atmospheric drag cancellation on parking orbit

Figure 3.2: Schematisation of the code for drag cancellation on parking orbit

- Transfer from parking orbit to target orbit with plane change

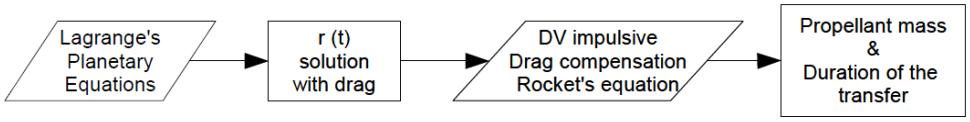

Figure 3.3: Schematisation of the code for transfer from PO to TO manoeuvre

- Re-entry from target orbit to an altitude of 50 km without plane change

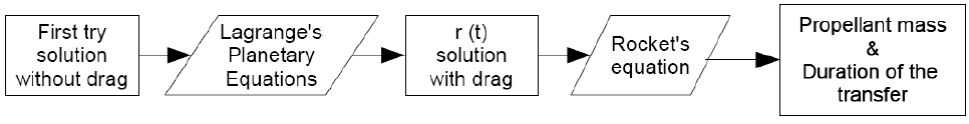

Figure 3.4: Schematisation of the code for re-entry manoeuvre

3.3.2 Manoeuvres for Electric Propulsion System

- Atmospheric drag cancellation on parking orbit

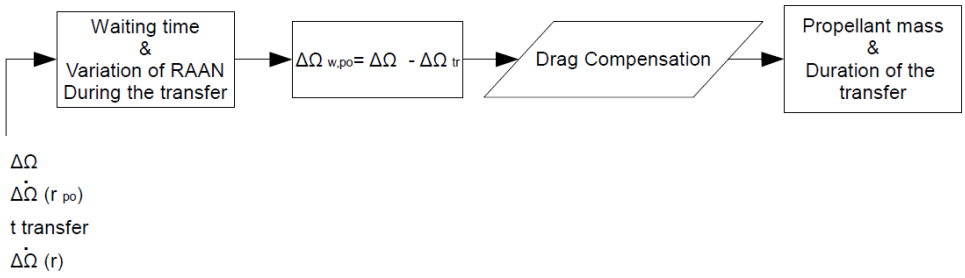

Figure 3.5: Schematisation of code for drag cancellation on parking orbit

- Re-entry from target orbit to an altitude of 50 km without plane change & Transfer from parking orbit to target orbit with plane change

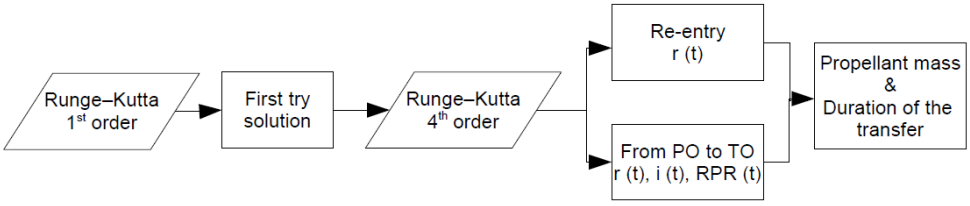

Figure 3.6: Schematisation of code for re-entry and transfer from PO to DO manoeuvres

Chapter 4

ADR Mission with Chemical Propulsion

The analysis is focused on the qualitative determination of the height and inclination of the parking orbit used to optimise the mass margin when the task is to remove 5 targets (Reference Number 20443, 21610, 22830, 23561, 23608), with orbital parameters described in tables (1.2). With the hypothesis that all the spacecraft are identical, it is possible to consider the dry mass as a constant.

The mass margin is:

$$MM = m_{del} - 5 \cdot m_d - \sum_{i=1}^{5} m_{p,tot}^{i} \tag{4.1}$$

The estimation of the propellant mass is committed to the Tsiolkowsky's equation. For implementation in the code, the equation is rearranged as:

$$m_{p,\alpha}^{i} = m_{fin,\alpha}^{i} \cdot \left[\exp\left(\frac{|\Delta V_{\alpha}^{i}|}{I_{sp} g} \right) - 1 \right] \tag{4.2}$$

where $m_{fin,\alpha}^{i}$ is the final mass at the end of the α–th manoeuvre[1].

This reformulation is useful because the estimation of the propellant mass for the whole mission is made backwards, or better starting with the re-entry until the atmospheric drag compensation manoeuvre. To estimate the propellant mass of the $\alpha - th$ manoeuvre it is necessary to know the quantity of propellant for the following manoeuvres.

A greater understanding of how perturbation effects determine the propellant mass necessary for the completion of the mission is realised looking at the relative precession rate (RPR) between parking orbit and target orbit. Assuming an initial RAAN (Right Ascension of the Ascending Node) of the spacecraft

[1]It is necessary to use the absolute value since for $r_{po} > r_{do}$ the same relations are still valid but they give negative ΔV.

is equal to 120°, the relative precession rate in reference to a generic orbit (representative of the five debris/target chosen) with orbital parameters of height h = 780 km and inclination i = 98.6°, is:

$$RPR = \dot{\Omega}_{po} - \dot{\Omega}_{do,ref} = -\frac{3}{2} \cdot J_2 \cdot R_E^2 \cdot \sqrt{\mu} \cdot \left(\frac{\cos i_{po}}{r_{po}^{5/2}} - \frac{\cos i_{do,ref}}{r_{do,ref}^{5/2}} \right) \tag{4.3}$$

For each manoeuvre, it is necessary to know the variation of the velocity and the final mass.

4.1 Manoeuvres Analysis

The main concept of the mission is characterised by a rendezvous performed by the spacecraft/chaser with the target and the re-entry. More propellant mass has to be spent for atmospheric drag compensation in the parking orbit during the waiting time to permit the alignment of the line of nodes. Manoeuvres are impulsive and are estimated the variation of the velocity and final mass, so that is possible to obtain the necessary propellant mass through Tsiolkowsky's equation. Besides, it is important to underline that the weight of the tanks is considered not dependent on the propellant mass to carry. Since the mass of the tank is around 4% of the dry mass of the spacecraft and its variation with propellant mass would be just a few decimal percent. This assumption is acceptable and simplifies the code, avoiding the need to create iterative processes with high computational costs.

4.1.1 Atmospheric Drag Compensation on Parking Orbit

For each target, from the flow mass rate definition, the propellant mass that contributes to the drag cancellation is:

$$m_{p,1} = \frac{D \cdot t_{w,po}}{I_{sp} \cdot g} = \frac{1/2 \cdot C_D A \cdot \rho(r_{po}) \cdot V_{po}^2}{I_{sp} \cdot g} \cdot t_{w,po} \tag{4.4}$$

Since the target rendezvous time is much lower than the waiting time for the the alignment of the line of nodes of parking orbit and target orbit, $t_{w,po}$ is uniquely determinated in the following way[2]:

$$t_{po} = \begin{cases} \frac{\Omega_{in,do} - \Omega_{in,po}}{\dot{\Omega}_{po} - \dot{\Omega}_{do,ref}} & \dot{\Omega}_{po} - \dot{\Omega}_{do,ref} > 0 \\ \frac{360° - (\Omega_{in,do} - \Omega_{in,po})}{\left|\dot{\Omega}_{po} - \dot{\Omega}_{do,ref}\right|} & \dot{\Omega}_{po} - \dot{\Omega}_{do,ref} < 0 \end{cases} \tag{4.5}$$

The chasers are set up in a stack of five spacecrafts and each one in turn performs the rendezvous. For this reason, the time for which a single chaser uses its engine is not the waiting time t_{po}, but the difference between its waiting time and the waiting time of the previous chaser.

[2] Assuming $\Omega_{in,po} = 120°$, per for each target is true that $\Omega_{in,do} - \Omega_{in,po} < 0$

4.1.2 Non-Coplanar Hohmann Transfer - Rendezvous -

This is characterised by a first impulse at the perigee, for a Hohmann transfer orbit inclined as the parking orbit, and a second impulse at the apogee for both circularisation and inclination change. It follows a combined manoeuvre where the Hohmann transfer and plane change collapses in only one manoeuvre.

The relations are:

$$\Delta V_{CP,P} = \sqrt{2\mu\left(\frac{1}{r_{po}} - \frac{1}{r_{po}+r_{to}}\right)} - \sqrt{\frac{\mu}{r_{po}}} \tag{4.6}$$

$$\Delta V_{CP,A} = \sqrt{V_{HT,A}^2 + V_{c,to}^2 - 2\cdot V_{HT,A}\cdot V_{c,to}\cdot\cos|i_{po}-i_{to}|} \tag{4.7}$$

The mass of the spacecraft/chaser at the end of the manoeuvre includes the propellant mass necessary to perform the successive manoeuvre. In this way:

$$m_{f,2} = m_d + m_{p,3} \longrightarrow Tsiolkowsky's\,equation \longrightarrow m_{p,2} \tag{4.8}$$

4.1.3 Re-entry

The re-entry is considered as a coplanar Hohmann transfer from the target orbit to the height of 50 km above the Earth's surface. It is important to underline that the second impulse at the perigee of the transfer orbit is null because the spacecraft uses the atmospheric drag to slow down the spacecraft. The variation of the velocity is:

$$\Delta V_3 = \sqrt{\frac{\mu}{r_{to}}} - \sqrt{2\mu\left(\frac{1}{r_{to}} - \frac{1}{r_{50km}+r_{to}}\right)} \tag{4.9}$$

The mass at the end of the manoeuvre includes the mass of the target that the spacecraft has to de-orbit:

$$m_{f,3} = m_d + m_D \longrightarrow Tsiolkowsky's\,equation \longrightarrow m_{p,3} \tag{4.10}$$

It is important to focus the attention on the fact that the propellant mass used during the re-entry is independent from r_{po} and i_{po}.

4.2 Atmospheric Drag Effects on Chemical Propulsion

When considering the atmospheric drag effect on the Hohmann transfer and de-orbit manoeuvres, it is possible to use the following model for air density as a function of altitude [14]. Whilst it is possible to find accurate values of density up to 200 km, for higher altitudes it is necessary to generate values using a model able to describe how density varies with altitude. With a hypothesis of:

- Atmosphere spherically symmetrical

- The air density does not vary with time
- Air density varies exponentially with distance 'r' from the Earth's centre
- Only tangential drag force is considered

It is possible to write:

$$\rho(r) = \rho_0 \cdot \exp \frac{(r_0 - r)}{H} \tag{4.11}$$

where ρ_0 is the density at the initial perigee point r_0 and H is the density scale height, defined as follows:

$$\frac{1}{H} = \frac{g}{R \cdot T} - \frac{2}{r_0} \tag{4.12}$$

where $R = 287.05\, J \cdot kg^{-1} \cdot K^{-1}$is the specific costant for dry air, $g = 9.81\, m/s^2$ is the standard gravity acceleration and, just in this chapter, $T = 700\, K$ is the air temperature (depending on solar activity and esposition), can be considered constant for $r > 200\, km$ [14].

4.2.1 Atmospheric Drag in Hohmann transfer

By taking a discrete trajectory and passing it through the eccentric anomaly, it is possible to obtain the position of the satellite as function of time. In each time range, the thrust used for drag compensation is considered constant and equal to the arithmetic average between the boundary values of the thrust in the time range considered.

The corresponding propellant mass in the generic $i - th$ step is:

$$m_p^i = \frac{\overline{T}^i \cdot \Delta t^i}{I_{sp} \cdot g} \tag{4.13}$$

where:

$$\overline{T}^i = \frac{T^{i+1} + T^i}{2} \tag{4.14}$$

By adding together all the contributions for the entire duration of the manoeuvres, it is possible to estimate the total propellant mass needed to compensate for the atmospheric drag during the Hohmann transfer.

4.2.2 Atmospheric Drag in Re-entry Manoeuvre

Atmospheric drag reduces the velocity of the satellite, therefore, it needs less propellant mass and equivalently ΔV to reach the desired height of the orbit.

It is possible to create an iterative method to understand how much propellant the satellite can save. As a first guess solution it is possible to use the trajectory obtained for an Hohmann transfer without the presence of atmospheric drag and then use the Lagrange's planetary equations linearised to

estimate the variation of semi-axis major (a) and eccentricity (e). At this point, if the satellite goes below the desired height ΔV has to be reduced and a new iteration is carried out until the satellite reaches the height but does not go below it, with a tolerance of 1 km.

Lagrange's planetary equations ([15, 16]) used are:

$$\frac{da}{dt} = \frac{2}{\pi}\sqrt{\frac{a^3}{\mu}} \int_0^{\pi} f_{drag}\sqrt{1 - e^2 \cdot \cos(E)}dE \tag{4.15}$$

$$\frac{de}{dt} = \frac{2}{\pi}\sqrt{\frac{a}{\mu}}(1 - e^2) \int_0^{\pi} f_{drag}\frac{\cos E(1 - e \cdot \cos E)}{\sqrt{1 - e^2 \cdot \cos E}}\sqrt{1 - e^2 \cdot \cos E}dE \tag{4.16}$$

Where:

$$f_{drag} = -\frac{1}{2} \cdot C_D A \cdot \rho(r) \cdot V^2(r) \tag{4.17}$$

For each iterative step:

$$a_{drag}(\Delta t) = a_{no-drag}(\Delta t) - \Delta a \tag{4.18}$$

$$e_{drag}(\Delta t) = e_{no-drag}(\Delta t) - \Delta e \tag{4.19}$$

Where the variations of the semi-axis major and eccentricity, due to the drag, are estimated by the linearisation of Lagrange's planetary equations:

$$\Delta a = \frac{da}{dt} \cdot \Delta t \longrightarrow \dot{a} = \dot{a}(f_{drag},\, a_{no-drag},\, e_{no-drag}) \tag{4.20}$$

$$\Delta e = \frac{de}{dt} \cdot \Delta t \longrightarrow \dot{e} = \dot{e}(f_{drag},\, a_{no-drag},\, e_{no-drag}) \tag{4.21}$$

A schematic representation of the iterative process is carried out in figure (4.1).

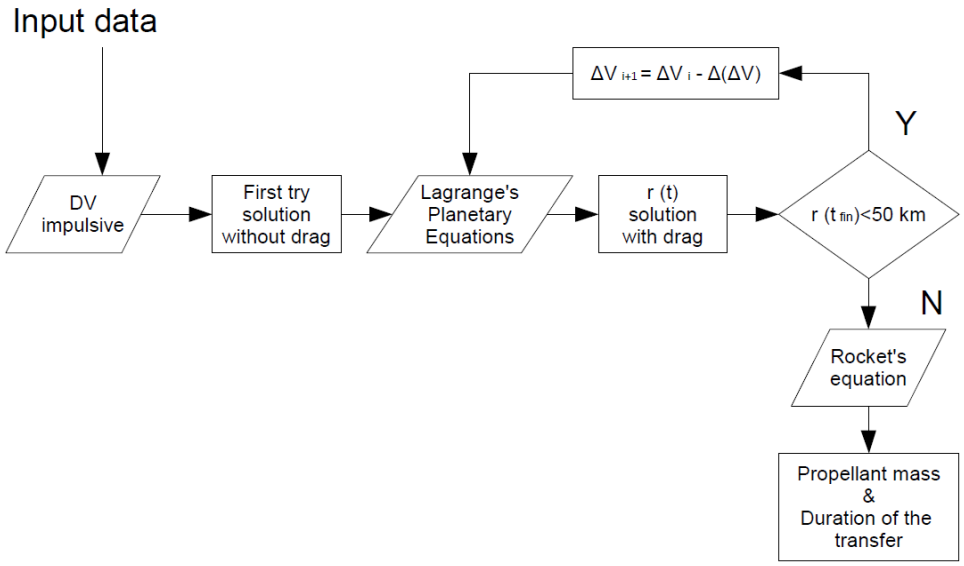

Figure 4.1: Iterative process scheme for re-entry manoeuvre

Chapter 5

ADR Mission with Electric Propulsion

In this chapter a discussion about a continuous low-thrust transfer between circular and inclined orbits is presented. Through the solution of Lagrange's planetary equations by a numerical integration with Runge-Kutta method of the fourth order, a simple model for describing the spacecraft motion is obtained. The validation of this model is made using the Edelbaum algorithm, which provides an analytical and optimal solution for this kind of problem, and with an approximated solution. As a preliminary project, a relative percentage error lower than 5-10% is sufficient.

After completing the model with atmospheric drag effects and gravitational perturbation (J2 effect), the results of the model are compared with those from chemical prolusion. Again, the mass of the tank is considered constant and is not dependent on the propellant mass. This hypothesis is acceptable since the mass of the tanks is about 1% of the dry mass of the spacecraft (about 10 kg) and variation of the dry mass due to variation of the propellant quantity is negligible.

5.1 Lagrange's Planetary Equations

The equation of motion for an orbit without perturbation, with distance r from the Earth's centre, is:

$$\ddot{\mathbf{r}} + \frac{\mu \mathbf{r}}{r^3} = 0 \tag{5.1}$$

Considering a perturbative force $\mathbf{f}$ for unit mass, the equation of motion becomes:

$$\ddot{\mathbf{r}} + \frac{\mu \mathbf{r}}{r^3} = \mathbf{f} \tag{5.2}$$

The orbit of a satellite can be conceived as an osculating ellipse, defined as the plane that contains the vector velocity and passes by the Earth's centre. The ellipse's size, shape and orientation vary due the perturbation acceleration effect.

The osculating plane is defined by the right ascension of the ascending node Ω and inclination i. Its position is specified in the orbital plan with an argument of periapsis ω, whilst the size and shape are described by semi-axis major a and eccentricity e. The position of the satellite on the osculating ellipse is given by the true anomaly θ and distance from the Earth's centre r.

The variation of the orbital parameters of the osculating orbit is described by Lagrange's planetary equations [17]:

$$\frac{da}{dt} = \frac{2a^2}{(\mu p)^{1/2}} \left[f_r e \sin\theta + f_t \left(1 + e\cos\theta\right) \right] \tag{5.3}$$

$$\frac{de}{dt} = \left(\frac{p}{\mu}\right)^{1/2} \left[f_r \sin\theta + f_t \left(\cos\theta + \cos E\right) \right] \tag{5.4}$$

$$\frac{di}{dt} = \frac{f_h r}{(\mu p)^{1/2}} \cos\left(\theta + \omega\right) \tag{5.5}$$

$$\frac{d\Omega}{dt} = \frac{f_h r}{(\mu p)^{1/2}} \frac{\sin\left(\theta + \omega\right)}{\sin i} \tag{5.6}$$

$$\frac{d\omega}{dt} = \frac{1}{e}\left(\frac{p}{\mu}\right)^{1/2} \left[-f_r \cos\theta + f_t \left(1 + \frac{r}{p}\right) \sin\theta \right] - \frac{f_h r}{(\mu p)^{1/2}} \cdot \cot i \cdot \sin(\theta + \omega) \tag{5.7}$$

where f_r is the radial component of the perturbation acceleration along the radius, f_t is the normal component to the radius and is in the osculating plane and f_h is the normal component to the orbital plane in direction of the angular momentum.

Also, the variation of the eccentric anomaly is:

$$\frac{dE}{dt} = \left(\frac{\mu}{a}\right)^{1/2} \frac{1}{r} + \frac{1}{e\sin E} \left[\frac{de}{dt} \cos E - r \frac{(da/dt)}{a^2} \right] \tag{5.8}$$

And parameters E, θ, r and p are defined with the common relations for elliptical orbit:

$$r = \frac{p}{1 + e\cos\theta} = a\left(1 - e\cos E\right) \tag{5.9}$$

$$p = a\left(1 - e^2\right) \tag{5.10}$$

$$\cos\theta = \frac{\cos E - e}{1 - e\cos E} \tag{5.11}$$

5.2 Validation of Numerical Method with Edelbaum Algorithm and Approximated Analytical Solution

The numerical model is based on the integration of Lagrange's planetary equations, specialised for transfers between inclined and circular orbits, using a Runge-Kutta method of the fourth order. The Edelbaum algorithm and an approximated analytical solution are also presented with the aim of validating the results obtained with the numerical method.

The transfer chosen as a reference for the validation is a rendezvous performed by the spacecraft from the parking orbit to the target orbit. These orbits are characterised by the following parameters:

- parking orbit: altitude $h = 300\,km$, inclination $i = 98.6°$ and initial RAAN iniziale dello spacecraft $RAAN_{in,po} = 120°$.
- target orbit: altitude $h = 757.2\,km$, inclination $i = 98.3°$ and initial RAAN $RAAN_{in,do} = 135.0506°$.

5.2.1 Edelbaum Algorithm

The Edelbaum algorithm provides an alternative method for optimising a transfer between circular and inclined orbits with a continuous low-thrust [9].Within each integration step, assuming a constant magnitude acceleration in the tangential and out-of-plane direction and the yaw thrust angle, whilst using the velocity as an independent variable, the Edelbaum algorithm linearises Lagrange's planetary equations. These equations describe the variation of orbital parameters due the external continuous force $f = [f_r,\, f_t,\, f_h]$, with radial, tangential and out-of-plane components.

For near-circular orbits, Lagrange's planetary equations are:

$$\frac{da}{dt} = \frac{2 \cdot a \cdot f_t}{V} \tag{5.12}$$

$$\frac{di}{dt} = \frac{\cos\vartheta \cdot f_h}{V} \tag{5.13}$$

$$\frac{d\vartheta}{dt} = n \tag{5.14}$$

Assuming only tangential and out-of-plane acceleration and if β is the out-of-plane or yaw thrust angle:

- $f_t = f \cdot \cos\beta$
- $f_h = f \cdot \sin\beta$
- $\vartheta = \vartheta^* + \omega = n \cdot t$

where ϑ^* is the true anomaly, ω is the argument of perigee and $n = \sqrt{(\mu/a^3)}$.

Averaging out the angular position in equation (5.13) and integrating with respect to ϑ with constant f, β and V, Lagrange's planetary equations are:

$$\frac{da}{dt} = \frac{2 \cdot a \cdot f_t}{V} \tag{5.15}$$

$$\frac{di}{dt} = \frac{2 \cdot f_h}{\pi \cdot V} \tag{5.16}$$

Using the velocity as independent variable and with continuous and constant acceleration, the problem is equivalent to minimise Δt and then the total ΔV (or propellant mass spent) since the engine is always on and no coasting arc are allowed. The objective becomes the determination of the yaw thrust angle (β in out-of-plane direction) to maximise the plane change in a given time range.

For $t \in [0,\, t_f]$ the algorithm is:

$$\Delta V = f \cdot t \tag{5.17}$$

$$\beta = \tan^{-1}\left[\frac{V_0 \cdot \sin\beta_0}{V_0 \cdot \cos\beta_0 - f \cdot t}\right] \tag{5.18}$$

$$V = \sqrt{V_0^2 - 2 \cdot V_0 \cdot f \cdot t \cdot \cos\beta_0 + f^2 \cdot t^2} \tag{5.19}$$

$$\Delta i = \frac{2}{\pi} \cdot \left[\tan^{-1}\left(\frac{f \cdot t - V_0 \cdot \cos\beta_0}{V_0 \cdot \sin\beta_0}\right) + \frac{\pi}{2} - \beta_0\right] \tag{5.20}$$

where:

$$\beta_0 = \tan^{-1}\left(\frac{\sin\frac{\pi}{2}\Delta i_f}{\frac{V_0}{V_f} - \cos\frac{\pi}{2}\Delta i_f}\right) \tag{5.21}$$

$$\Delta i_f = |i_f - i_i| \tag{5.22}$$

$$t_f = \frac{\Delta V_{tot}}{f} = \frac{V_f - V_i}{f} \tag{5.23}$$

The algorithm is valid regardless of whether the transfer is at a higher or lower orbit; the operation limit with a maximum difference of inclination is about 114.591°.

For the examined transfer, plots 5.1 and 5.2 represent the results obtained with the Edelbaum algorithm.

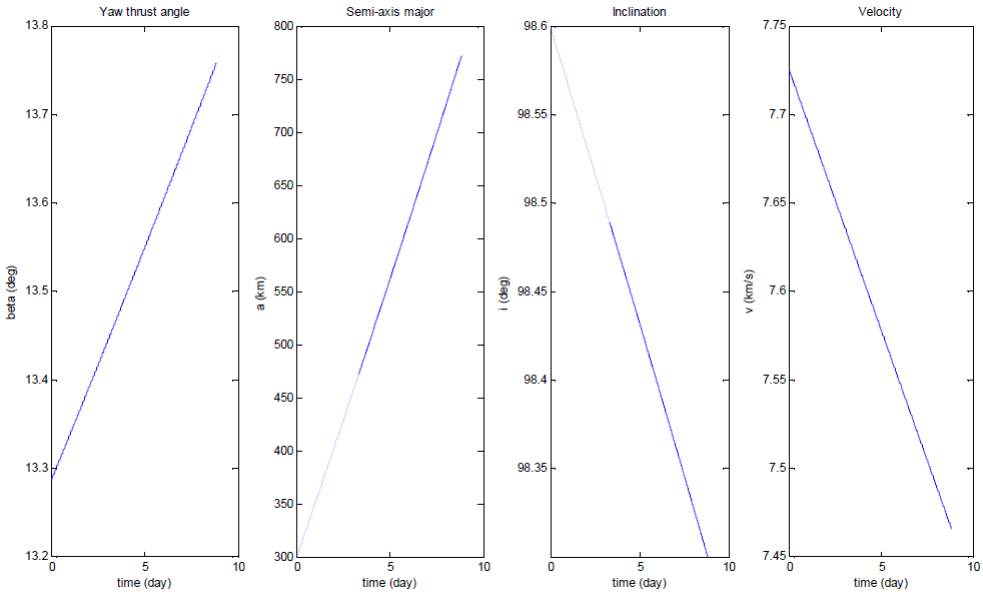

Figure 5.1: Orbital parameters as function of the time - Edelbaum algorithm

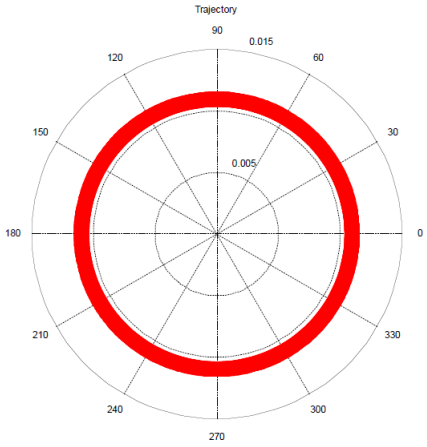

Figure 5.2: Trajectory in polar coordinates

5.2.2 Analytical Approximated Solution

The following model is a simplified approach for considering a transfer between two circular orbits, considering the variation of the specific energy of the spacecraft when a continuous low-thrust is applied.

For a circular orbit with radius r, the specific energy ξ is:

$$\xi = -\frac{\mu}{2r} \tag{5.24}$$

The derivative of specific energy with respect to the time is:

$$\frac{d\xi}{dt} = \frac{\mu}{2r^2} \cdot \frac{dr}{dt} \tag{5.25}$$

This is equal to the power, therefore:

$$\frac{d\xi}{dt} = \frac{T \cdot V}{m} \longrightarrow \frac{\mu}{2r^2} \cdot \frac{dr}{dt} = \frac{T}{m} \cdot \sqrt{\frac{\mu}{r}} \tag{5.26}$$

The hypothesis of the model is:

- The mass of the spacecraft decrease with the time:

$$m(t) = m_{in} - \dot{m} \cdot t \tag{5.27}$$

where $\dot{m}$ is the mass flow rate estimated as:

$$\dot{m} = \frac{T}{u_{eq}} \tag{5.28}$$

with u_{eq} exhaust velocity, that for the generical selected engine is equal to $u_{eq} = I_{sp} \cdot g \cong 12\, km/s$.

- Since the thrust is constant (in accordance with the other models), the thrust will decrease with time as well. In this case, it is not an absurdity to consider the acceleration thrust constant and equal to the initial one, because the mass varies slightly during the transfer.

$$f_T = f_{T,in} = \frac{T}{m_{in}} \tag{5.29}$$

As a consequence of this assumption, the mass flow rate is constant and equal to:

$$\dot{m} = \frac{T}{u_{eq}} = \frac{m_{in}}{u_{eq}} \cdot f_T \tag{5.30}$$

Integrating between the altitude of the parking orbit r_{po} at initial time $t = 0$, and a generic altitude r at time t, it follows:

$$\int_{r_{po}}^{r} r^{-3/2} dr = \frac{2 \cdot T_{in}}{\sqrt{\mu}} \int_{0}^{t} \frac{dt}{m_{in} - \dot{m} \cdot t} \tag{5.31}$$

The analytical approximated solution that describes the variation of the altitude with time is:

$$r(t) = \left[\frac{u_{eq}}{\sqrt{\mu}} \log \left(\frac{m_{in} - \dot{m} \cdot t}{m_{in}} \right) + \frac{1}{\sqrt{r_{po}}} \right]^{-2} \tag{5.32}$$

The duration of the transfer is obtained by putting the altitude of the target orbit as $r_{to} = r(t_{tr})$:

$$t_{tr} = \frac{1}{\dot{m}} \left\{ m_{in} - m_{in} \cdot \exp \left[\frac{u_{eq}}{\sqrt{\mu}} \left(\frac{1}{\sqrt{r_{to}}} - \frac{1}{\sqrt{r_{po}}} \right) \right] \right\} \tag{5.33}$$

In this way it is possible to calculate the total propellant mass necessary for the transfer as follows:

$$m_p = \dot{m} \cdot t_{tr} = m_{in} - m_{in} \cdot \exp \left[\frac{u_{eq}}{\sqrt{\mu}} \left(\frac{1}{\sqrt{r_{to}}} - \frac{1}{\sqrt{r_{po}}} \right) \right] \tag{5.34}$$

5.2.3 Comparison between Models

The aim of this section is to make a comparison between the models to ensure their reliability.

Since the approximated solution does not take into account the plane changes the transfer is considered coplanar. Results obtained with the numerical model are compared with the Edelbaum algorithm and the analytically approximated solution.

Model	$m_{p,tot}(kg)$	$t_{tot}(day)$
Edelbaum Algorithm	18.0950	8.5903
Analytical Solution	18.3017	8.4959
Numerical Model	18.0960	8.5897

Table 5.1: Numerical model validation - Coplanar transfer

The relative percentage error is:

	$\Delta m(\%)$	$\Delta t(\%)$
NM vs EA	< 0.1	< 0.1
NM vs AS	1.12	1.10

Table 5.2: Relative percentage error - Coplanar Transfer

The three methods are in agreement with each other, providing the same results for the coplanar transfer with a relative percentage error lower than 0.1 % for the Edelbaum algorithm and about 1% for the analytically approximated solution. The higher capability of the Edelbaum algorithm in finding the optimal solution is evident when the transfer is no longer coplanar. Since the method with the analytically approximated solution does not consider non-coplanar transfer, the comparison is just made with the Edelbaum algorithm.

Model	$m_{p,tot}(kg)$	$t_{tot}(day)$
Edelbaum Algorithm	18.6104	8.8349
Numerical Model	18.6502	8.9758

Table 5.3: Numerical model validation - Non-coplanar transfer

	$\Delta m(\%)$	$\Delta t(\%)$
NM vs EA	<1	1.60

Table 5.4: Relative percentage error - Coplanar Transfer

Also, in this case the relative percentage error is about 1%, confirming the consistence of the numerical model implemented in the code.

5.3 Earth's Gravitational Perturbation Effect (J_2)

The introduction of the gravitational perturbation effect J_2 leads to the necessity to consider extra waiting time for the spacecraft in the parking orbit to make it possible for the line of nodes to be aligned. During the waiting time, due to the atmospheric drag it is necessary to perform a drag cancellation manoeuvre.

Whether or not the duration of the transfer is much lower than the waiting time in the parking orbit for the alignment of the apses line (figure 5.3) for chemical propulsion, this is no longer true for electric propulsion. It is necessary to consider that the alignment is achieved also during the transfer (figure 5.4), therefore with a RPR as a function of the orbit height.

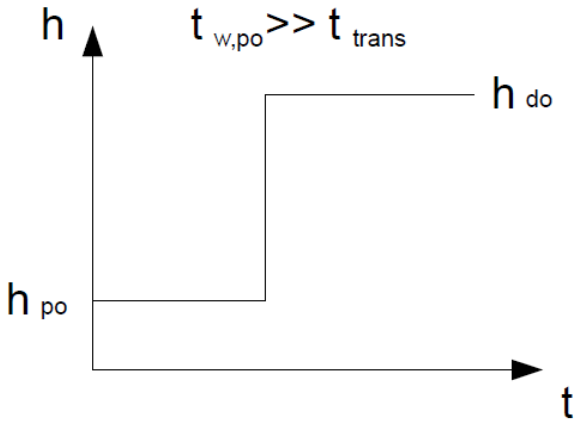

Figure 5.3: Schematisation of the transfer in time - Chemical Propulsion

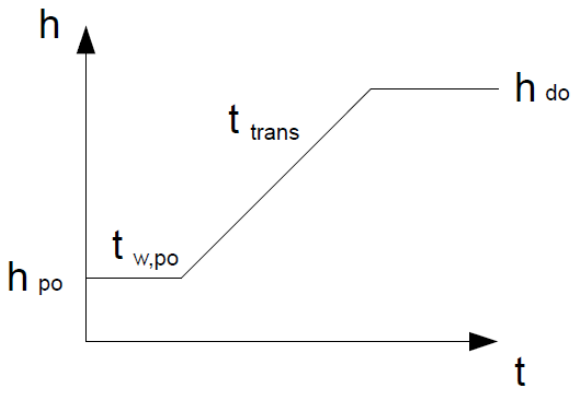

Figure 5.4: Schematisation of the transfer in time - Electric Propulsion

The difference between the initial RAANs of the parking orbit and target orbit is cancelled whilst waiting in the parking orbit and during the transfer:

$$\Delta\Omega = \Delta\Omega_w + \Delta\Omega_{trans} \tag{5.35}$$

and in terms of time:

$$t_{w,po} = \frac{\Delta\Omega_w}{\Delta\dot{\Omega}_w} \neq f(r) \tag{5.36}$$

$$t_{trans} = \frac{\Delta\Omega_{trans}}{\Delta\dot{\Omega}_{trans}} = f(r) \tag{5.37}$$

Knowing t_{trans} and $\Delta\dot{\Omega}_{trans}$ (assumed constant in each time range) from the numerical integration and the relative precession rates from (2.3), it is possible to estimate the waiting time for the parking orbit and therefore the propellant mass necessary to compensate the atmospheric drag.

5.3.1 Comparison with Edelbaum Algorithm

For electric propulsion, a process of validation is made by comparing the solutions of the Edelbaum algorithm and the model which provides the numerical integration of Lagrange's planetary equations. For the non-coplanar transfer, the results are:

	$m_{p,po2to}(kg)$	$t_{po2to}(day)$	$m_{p,J2}(kg)$	$t_{w,po}(day)$	$m_{tot}(kg)$	$t_{tot}(day)$
EA	18.6101	8.8349	1.6877	44.9003	20.2978	53.7352
NI	18.6644	8.9763	1.6889	44.9335	20.3533	53.9098

Table 5.5: Validation of Numerical Methods

	propellant mass	duration of the transfer
$\Delta e\,(\%)$	<1	<1

Table 5.6: Relative Percentage Error

With a relative percentage error of less than 1%, it is possible to consider the model validated.

5.4 Introduction of Atmospheric Drag

As with the impulsive case, the atmospheric drag effect is considered for the reentry and rendezvous manoeuvres. The atmospheric drag effect is introduced separately in the numerical model and approximated analytical solution and is used in the final validation process.

- Numerical Integration of Lagrange's Planetary equations

The numerical integration is carried out including the effect of atmospheric drag, in the same way as the case without drag. Rates of change due to the drag can be added to the thrust induced rates of change. Lagrange's planetary equations, for drag induced rates of change [15, 16] are:

$$\frac{da}{dt} = \frac{2}{\pi}\sqrt{\frac{a^3}{\mu}}\int_0^{\pi} f_{drag}\cdot\sqrt{1-e^2\cos^2 E}dE \tag{5.38}$$

$$\frac{de}{dt} = \frac{2}{\pi}\sqrt{\frac{a}{\mu}}(1-e^2)\int_0^{\pi} f_{drag}\cdot\frac{\cos E(1-e\cos E)}{\sqrt{1-e^2\cos^2 E}}dE \tag{5.39}$$

- Approximated Analytical Solution

Considering atmospheric drag means that the derivative of the specific energy of the spacecraft is:

$$\frac{dE}{dt} = \frac{(T-D)\cdot V}{m} \longrightarrow \frac{\mu}{2r^2}\cdot\frac{dr}{dt} = \frac{T-D}{m}\cdot\sqrt{\frac{\mu}{r}} \tag{5.40}$$

where the drag is:

$$\frac{D}{m} = \frac{1}{2}\cdot C_D A\cdot\rho(r)\cdot V^2 \tag{5.41}$$

Assuming the same hypothesis as in paragraph 5.2.2 and using the exponential model for air density, after some mathematical manipulations, it is possible to obtain:

$$\frac{dr}{dt} = \left[\frac{2\cdot T_{in}}{m_{in}-\dot{m}\cdot t} - \mu C_D A\rho_0\cdot\frac{\exp\left(\frac{r_0-r}{H}\right)}{r}\right]\cdot\sqrt{\frac{r^3}{\mu}} \tag{5.42}$$

For the complexity of the equation, it's necessary to integrate numerically:

$$r_{i+1} = r_i + \left[\frac{2 \cdot T_{in}}{m_{in} - \dot{m} \cdot t_i} - \mu C_D A \rho_0 \cdot \frac{\exp\left(\frac{r_0 - r_i}{H}\right)}{r_i} \right] \cdot \sqrt{\frac{r_i^3}{\mu}} \cdot \Delta t \qquad (5.43)$$

5.4.1 Validation with Approximated Analytical Solution

Although it has been defined as analytical, the introduction of the atmospheric drag effect leads the necessity to integrate the differential equation obtained numerically. However, the validation of the numerical model is made by comparing the results of this solution.

The following table (5.7) provides information about propellant mass and duration of the transfer, emphasising the presence of a quantity of additional propellant mass and time with respect to the solution, that neglected the atmospheric drag.

Model	$m_{p,tot}(kg)$	$add.\ mass(kg)$	$t_{tot}(day)$	$add.\ time(day)$
Analytical Solution	18.3104	+0.0087	8.5028	+0.0069
Numerical Method	18.6623	+0.0121	8.9760	+0.0002

Table 5.7: Numerical Method Validation

The relative percentage error is:

	$\Delta m(\%)$	$\Delta t(\%)$
NM vs AS	1.92	5.57

Table 5.8: Relative percentage error

Although the error is higher, for a preliminary design, it is possible to consider the model validated.

5.4.2 Comparison

The validation of the model provides the solution of the problem of numerically integrating Lagrange's planetary equations including atmospheric drag, but neglecting the gravitational perturbation of the Earth (J2 effects). In the following tables, the results of a simulation that consider a transfer between two inclined circular orbits (from parking orbit to target orbit) and a re-entry manoeuvre to the height of 50 km are reported. The aim of the simulation is to compare it with the solution without the atmospheric drag.

A useful comparison with the model that not consider the drag in terms of time and propellant mass used for the manoeuvres, let to understand that during the re-entry the effects of drag help the spacecraft to decelerate, even if

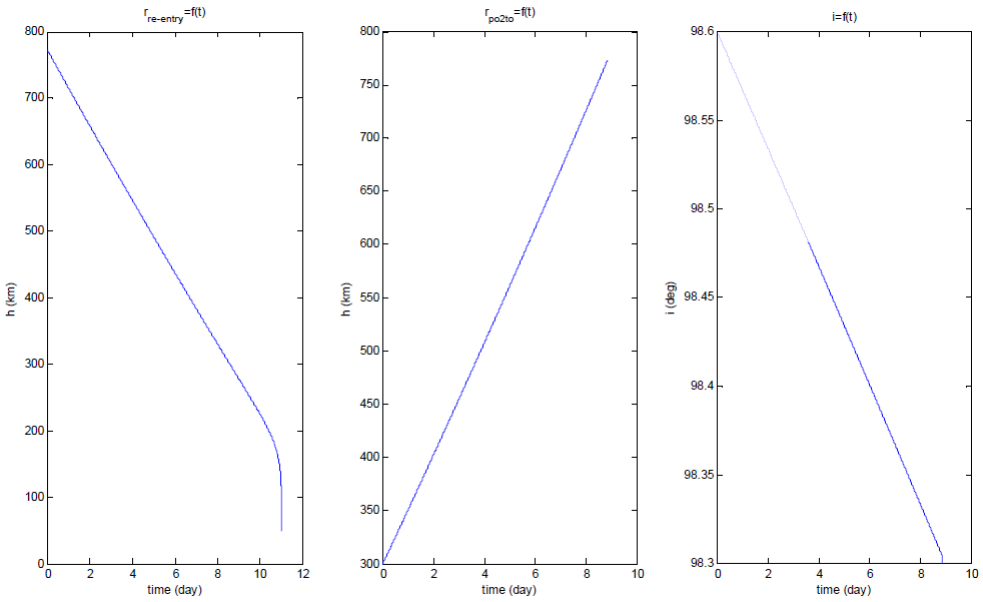

Figure 5.6: Numerical Integration of Lagrange's planetary equations - With drag effects

it is not true during the apogee raising. Overall, there is a saving of propellant mass and duration of the transfers, how happened for the chemical propulsion.

Model	$m_{p,re-entry}(kg)$	$t_{re-entry}(day)$	$m_{p,po2to}(kg)$	$t_{po2tp}(day)$
Without Drag	83.9323	13.5014	18.6501	8.9758
With Drag	68.4190	11.0060	18.6623	8.9760

Table 5.9: Comparison between transfers with or without drag effects

Model	$m_{p,tot}(kg)$	$t_{tot}(day)$
Without Drag	102.5825	22.4772
With Drag	87.0821	19.9821

Figure 5.5: Total mass and total duration

The figures 5.7,5.6 represent the height of the spacecraft during the re-entry and the apogee rising, and the inclination as functions of the time for the examined model and that one that neglected the atmospheric drag. It is evident as in the re-entry phase the duration is reduced and for low altitudes the atmospheric drag effect de-orbits the spacecraft quicker.

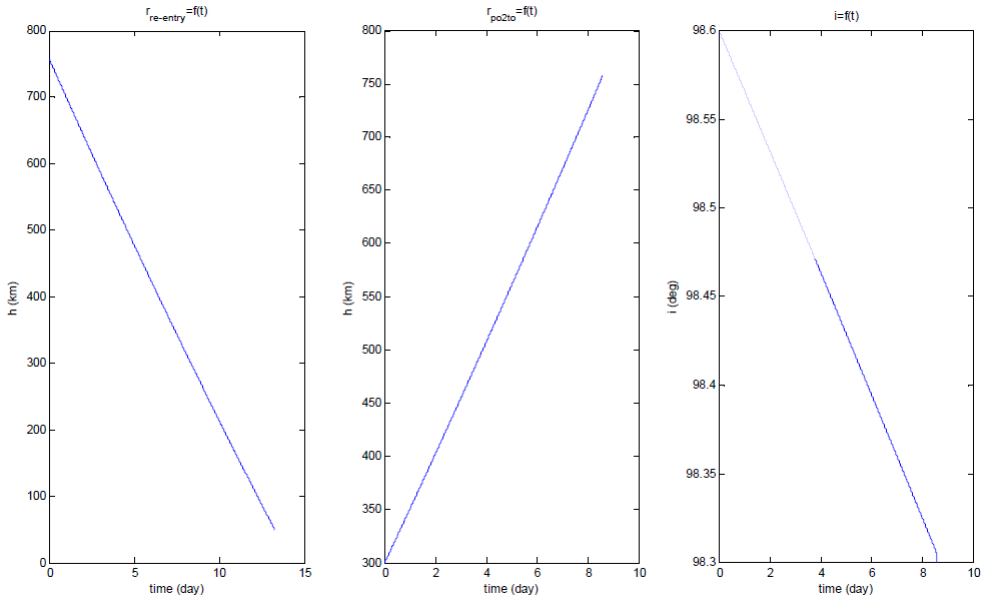

Figure 5.7: Numerical Integration of Lagrange's planetary equations - Without drag effects

5.5 Sensitivity Tests

As preliminary design, the study gives an initial prospective of the possible solutions for the examined problem, without the claim to find the best one. For this reason, it is possible to carry out an analysis where results are observed when input data are modified. The aim is to highlight the aspects where a higher effort should be given for a successive and more detailed design phase.

The variation is applied on the following input parameters:

- Dry mass
- Specific Impulse
- Initial RAAN

5.5.1 Sensitivity Test on Dry Mass

Reduction of the dry mass of a spacecraft is always one of the most challanging tasks during the project design. If the advantages obtained reducing the dry mass are significant, it is necessary to make an effort in this direction otherwise it is possible to focus the attention on other aspects.

The dry mass of the electric spacecraft is reduced by 20%. In a successive and detailed design, it may be necessary to estimate more precisely the mass budget and reduce the dry mass of the spacecraft.

5.5.2 Sensitivity Test on Specific Impulse

A high performance spacecraft can introduce improvements on the whole mission. A high specific impulse engine is used and table (5.10) presents reference values concerning the main characteristics for typical electric engines.

	PPT	SPT	Ion Thruster	FEEP
Propellant	Teflon	Xe	Xe	Caesium
$P_R(kW)$	0.001 - 0.025	0.15 - 1.5	0.4 - 2.0	0.00001 - 0.12
$T(mN)$	0.01 - 1	40 - 200	15 - 200	0.001 - 5
$I_{sp}(s)$	300 - 1000	1500 - 1700	1800 - 3500	5000 - 10000
$\eta(\%)$	20	48	60 - 70	80

Table 5.10: References for high performance electric engines[18]

where: PPT is Pulsed Plasma Thruster, SPT is Stationary Plasma Thruster and FEEP is Field Emission Electric Propulsion. The requested input power is P_R, the efficiency η is the thruster power output-power plant input power ratio. PPU is the Power Processing Unit.

The choice is on an ion thruster engine (NSTAR, NASA's Ion thruster). Its characteristics are:

	NSTAR Ion Thruster
$P_R(kW)$	2.3
$I_{sp}(s)$	3300
$T(mN)$	92

Table 5.11: NSTAR Engine [19]

A high performance engine introduces modification on the whole system, in terms of requested power, dry mass, dimension. Assuming the same geometry used for the low performance spacecraft, the high performance one has the following parameters:

System	$m_d(kg)$	$I_{sp}(s)$	C_D	$A(m^2)$
Electric	404.5	3300	2.2	4

Table 5.12: High performance spacecraft

The dry mass of this high performance chaser is estimated with a simple model for spacecraft mass estimation that it is discussed in detail in appendix A.

5.5.3 Sensitivity Test on Initial RAAN

For low altitudes, the waiting time on the parking orbit for the alignment of the line of nodes implies significant quantity of propellant mass for drag cancellation manoeuvres.

With the aim to reduce the propellant mass used and time spent on the parking orbit for the drag compensation manoeuvre, the possibility of having different initial RAANs for each target seems to be interesting. Since the variation of the right ascension of the ascending node during the transfer is always between 1 and 20°, the initial RAAN chosen for each spacecraft is the initial RAAN of the target minus 20°. For each spacecraft chaser:

$$\Omega_{in,s/c} = \Omega_{in,T} - 20^\circ \tag{5.44}$$

An alternative solution is suggested by the asymmetric behaviour of the mass margin for inclination close to 98°. If the initial RAAN of the parking orbit is lower than the initial RAAN of the target orbit and the relative precession rate is negative, the angle that has to be swept during the alignment is the explementary of the difference between the initial RAANs. Thus, if the difference is small, the waiting time and correspondingly the propellant mass is high.

It is possible to avoid this waste if propellant mass choosing an initial RAAN of the spacecraft higher than the initial RAAN of the target when the relative precession rate is negative. In this way, for each spacecraft chaser:

$$\begin{array}{ll} \Omega_{in,s/c} = \Omega_{in,T} - 20^\circ & \dot{\Omega}_{po} - \dot{\Omega}_{to} > 0 \\ \Omega_{in,s/c} = \Omega_{in,T} + 20^\circ & \dot{\Omega}_{po} - \dot{\Omega}_{to} < 0 \end{array} \tag{5.45}$$

Chapter 6

ADR Mission with Hybrid Propulsion

The electric propulsion may not introduce benefits in terms of mass margin, since the dry mass of the spacecraft is significantly increased. Also, this propulsion system reduces the accuracy in the prediction of the re-entry point in atmosphere, since the altitude quickly and unpredictably decreases due the atmospheric drag.

For these reasons, alternative mission architectures are proposed leading to hybrid propulsion systems. The idea is to use electric propulsion to perform the rendez-vous with the target in its orbit and transport it again in the parking orbit, whilst the chemical propulsion system is used for the target re-entry in the atmosphere. Thus, it is possible to control the re-entry point; for instance, in an uninhabited area in the Pacific, saving propellant mass using the more suitable propulsion system, depending on the manoeuvre.

New configurations of spacecraft are conceived in this section. The denomination of the interested spacecraft for the analysed mission architectures are:

- Bus for fuel resupply on parking orbit (B)
- Electrically propelled Shuttle (S)
- Chemically propelled Tug (T)

6.1 Code Documentation for Hybrid Propulsion Systems

As for chemical and electric propulsion systems, the intent is to underline the user's knowledge necessary to obtain results.

Launcher, debris and spacecraft characteristics are requested also with a confident knowledge about operative environment and equations for describing

all the manoeuvres. The right ascension of the ascending node adjustment is another typology of manoeuvre added for controlling the RAAN of the orbit.

An important key assumption concernes the drag coefficient for the hybrid spacecraft. Generally launcher upper stages and orbiting spacecraft have $l/d = 2 \div 5$. As first estimation, the drag coefficient is $C_D = 2(1 + 0.44r)$. When a standard value is needed, as chosen for this study, it is possible to use $C_D = 2.2$ [21].

6.2 Mission Architectures for Hybrid Propulsion Systems

The concept of hybrid propulsion system lets to conceive different missions. In this section, mission architectures are described for the achievement of the aim of the mission. The main mission architecture presented are:

- Hybrid Spacecraft: the spacecraft has both chemical and electric propulsion systems
- Hybrid System: the spacecraft has two sub-spacecraft, an electrically propelled shuttle and a chemically propelled tug, working together in the initial configuration and independently during the mission.
- Hybrid System with Bus: an orbiting station, or bus, with an electric propulsion engine is on the parking orbit, resupplies the shuttle and carries the tugs.

For each architecture characteristics of the spacecraft are presented, describing the main manoeuvres with a schematic and conceptual representation of the mission. The qualitative identification of the parking orbit will be made just for the most effective configurations for the achievement of the aim of the study.

Hybrid spacecraft dry mass estimation is discussed in appendix A.

6.2.1 Hybrid Spacecraft

Chemical and electric propulsion systems are combined in the same spacecraft, denominated hybrid. Each target is related to one hybrid spacecraft that performs a rendezvous with the debris and de-orbits it to the parking orbit with the electric system. The final burn for the re-entry is demanded to the chemical propulsion system.

The characteristics of the spacecraft are:

System	$m_d(kg)$	$I_{sp,ch}(s)$	$I_{sp,el}(s)$	C_D	$A\,(m^2)$
Hybrid	462.4	312	1640	2.2	4

Table 6.1: Hybrid spacecraft parameters

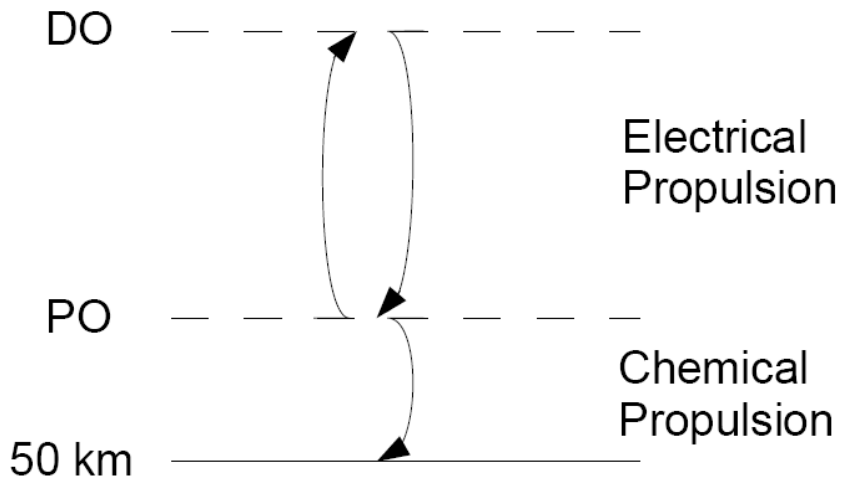

Figure 6.1: Mission architecture - Hybrid Spacecraft

Each spacecraft has to perform the following manoeuvres:

- With electric propulsion: atmospheric drag compensation in the parking orbit during the waiting time for the alignment of line of nodes, rendezvous with the debris considering the plane change, re-entry to the parking orbit.
- With chemical propulsion: re-entry from the parking orbit

6.2.2 Hybrid System

The hybrid system consists in using two spacecraft: an electrically propelled shuttle and a chemically propelled tug, that can work jointly or independently. The aim of the electric shuttle is the rendezvous with the debris and to carry it to the parking orbit, where the chemical tug performs the atmospheric re-entry. Another differentiation is made considering the re-entry with the chemical tug from the debris orbit.

6.2.2.1 Single Debris Recovery

Each debris is removed separately and when the electric shuttle comes brings one of them back to the parking orbit, a tug is detached and performs the re-entry. The initial configuration of the hybrid system is the composition of the electric shuttle and five tugs, jointed with the shuttle by a dispenser.

Robotic arm and dispenser are defined symbolically as shown in figure 6.2.

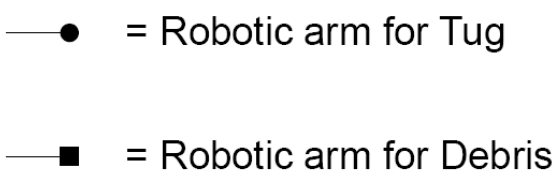

Figura 6.2: Legend

The hybrid system configuration is:

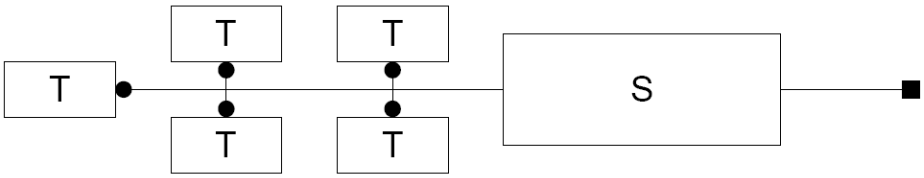

Figura 6.3: Spacecraft configuration for single debris recovery

The characteristics of the electric shuttle are:

System	$m_d(kg)$	$I_{sp,el}(s)$	C_D	$A\,(m^2)$
Electric	790	1640	2.2	4

Table 6.2: Electric shuttle

By differentiating the re-entry from parking orbit or target orbit, the characteristics of the chemical tug are:

System	$m_d(kg)$	$I_{sp,ch}(s)$	C_D	$A\,(m^2)$
Chemical - Re-entry from PO	365	312	2.2	4
Chemical - Re-entry from DO	455	312	2.2	4

Table 6.3: Chemical tug

The schematic concept of the mission can be summarised as shown in figure 6.4.

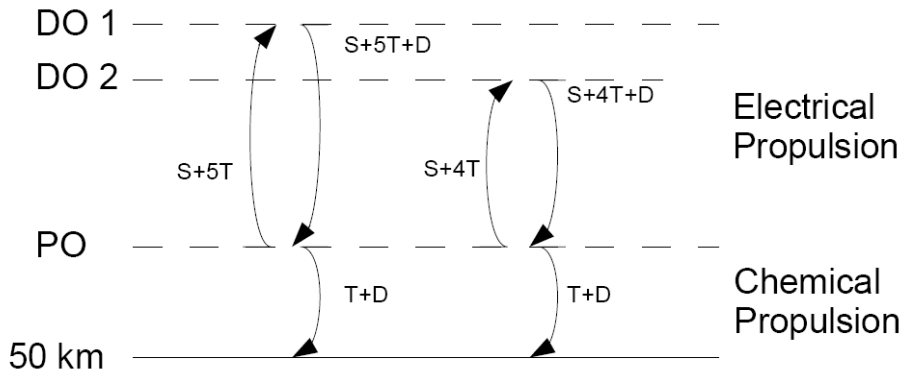

Figure 6.4: Mission architecture – Hybrid system, single debris recovery, re-entry from PO

6.2.2.2 Cascade Debris Recovery

In this configuration the shuttle does not come back in the parking orbit; when it reaches the debris with the highest altitude, the shuttle recovers all the debris in cascade and in a descending order sorted by orbit altitude. When the shuttle is back in the parking orbit, a single tug re-entries all the debris.

The initial configuration of the hybrid system is:

Figura 6.5: Spacecraft configuration for cascade debris recovery

The characteristics of the electric shuttle are:

System	$m_d(kg)$	$I_{sp,el}(s)$	C_D	$A\,(m^2)$
Electric	1200	1640	2.2	6

Table 6.4: Electric shuttle

Whilst the characteristics of the tug are:

System	$m_d(kg)$	$I_{sp,ch}(s)$	C_D	$A\,(m^2)$
Chemical	755	312	2.2	5

Table 6.5: Chemical tug

A schematic representation of the mission concept is reported in figure 6.6.

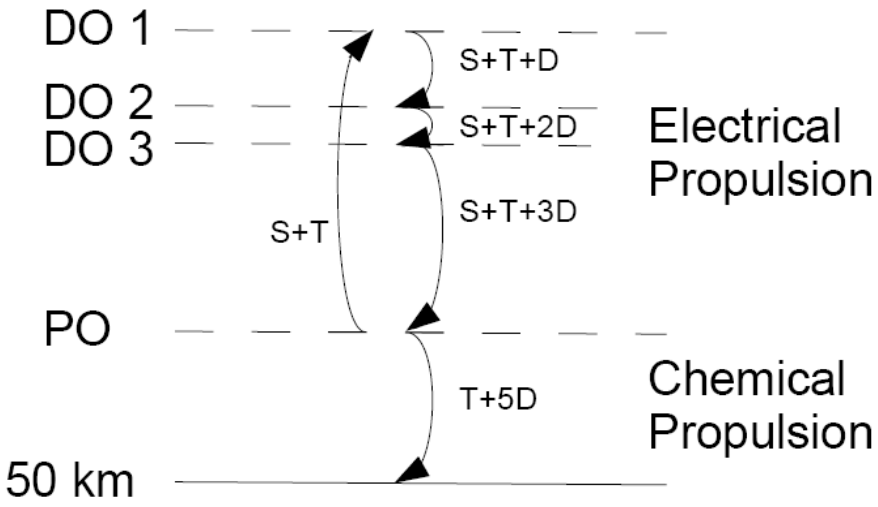

Figure 6.6: Mission architecture - Hybrid system, cascade debris recovery.

6.2.3 Hybrid System with Orbiting Bus

The hybrid system with orbiting bus configuration consists in a electrically propelled bus in the parking orbit, an electric shuttle and a chemical tug. The aim of the shuttle and tugs is the same described in the previous section, but the presence of the bus allows the shuttle to do not carry the tugs that are jointed to the bus by a dispenser, and the propellant mass not necessary for the successive manoeuvres, since the bus will provide to the fuel resupply.

The characteristics of the bus are:

System	$m_d(kg)$	$I_{sp,el}(s)$	C_D	$A(m^2)$
Electric	980	1640	2.2	6

Table 6.6: Electric bus

If the re-entry is performed separately (the shuttle recovers one debris and returns to the parking orbit) or in a unique re-entry manoeuvre (the shuttle collects all the debris before to come back in the parking orbit) the differentiation is in multiple or single tug, respectively .

6.2.3.1 Multiple Tugs

The re-entry can be performed from the debris orbit or parking orbit. The configuration of the spacecraft in the architecture that considers the re-entry from the parking orbit is in figure 6.7.

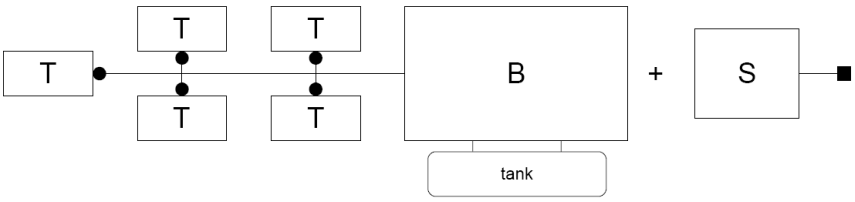

Figura 6.7: Spacecraft configuration for multiple tugs

If the re-entry is performed from the parking orbit or target orbit, the electric shuttle needs another robotic arm for transporting the tug to the debris orbit. Its characteristics are:

System	$m_d(kg)$	$I_{sp,el}(s)$	C_D	$A(m^2)$
Electric - Re-entry from PO	382.3	1640	2.2	4
Electric - Re-entry from DO	442.3	1640	2.2	4

Table 6.7: Electric shuttle

For the tugs:

System	$m_d(kg)$	$I_{sp,ch}(s)$	C_D	$A\,(m^2)$
Chemical - Re-entry from PO	365	312	2.2	4
Chemical- Re-entry from DO	455	312	2.2	4

Table 6.8: Chemical tug

The schematic representation of the mission is in figure 6.8.

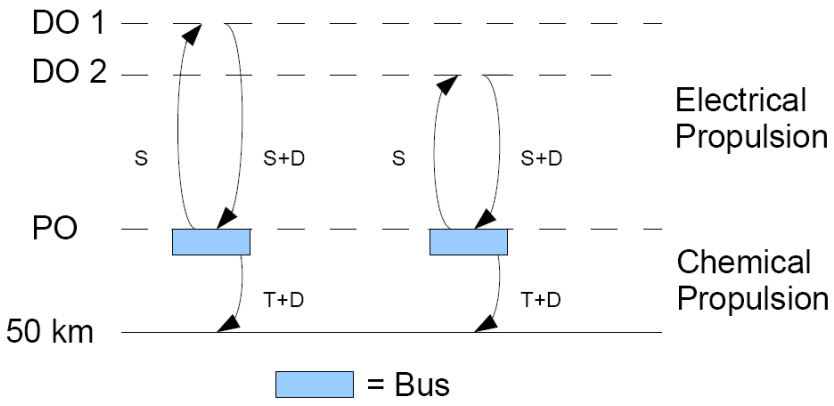

Figure 6.8: Mission architecture – Hybrid system and bus, multiple tugs.

6.2.3.2 Single Tug

After the shuttle has de-orbited all the debris in the parking orbit and docked them to the bus, a single chemical tug performs the re-entry of all the targets.

The initial configuration of the hybrid system is in figure 6.9.

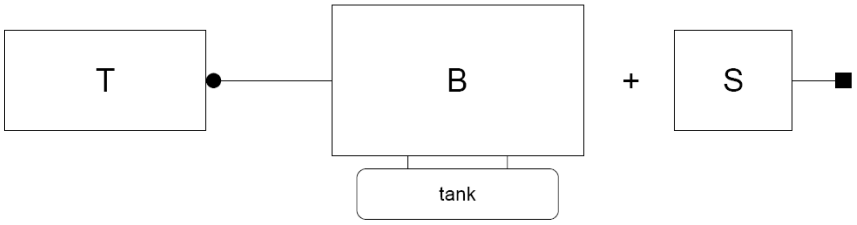

Figura 6.9: Spacecraft configuration for single tug

In this case the characteristics of the shuttle are:

System	$m_d(kg)$	$I_{sp,el}(s)$	C_D	$A(m^2)$
Electric	382.3	1640	2.2	4

Table 6.9: Electric shuttle

The characteristics of the tug are:

System	$m_d(kg)$	$I_{sp,ch}(s)$	C_D	$A\,(m^2)$
Chemical	755	312	2.2	5

Table 6.10: Chemical tug

The schematic representation of the mission is in figure 6.10.

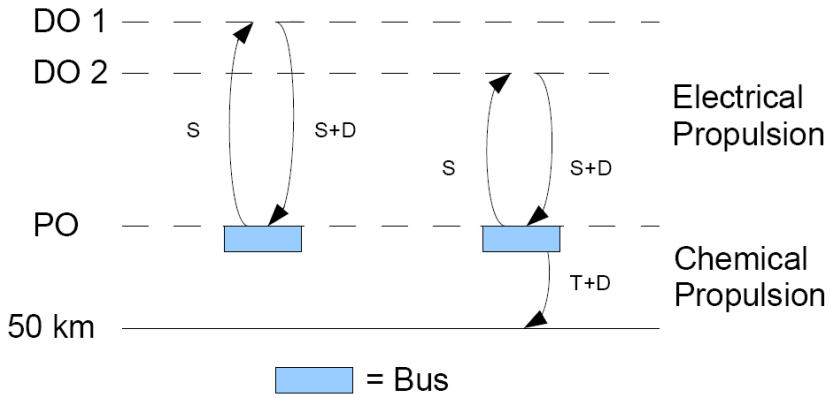

Figure 6.10: Mission architecture – Hybrid system and bus, single tug.

Chapter 7

Results and Discussion

Results are differentiated for each propulsion system by showing the mass margin and the relative precession rate as function of altitude and inclination of the parking orbit. The plots are discussed and a comparison between the solutions is made. Also, a discussion is presented to highlight the most important key assumptions, the architecture and selection options.

7.1 Qualitative Identification of the Parking Orbit with Chemical Propulsion

The analysis is carried out by varying height and inclination of the parking orbit and by calculating the corresponding mass margin. The figure (7.1) presents the RPR as a function of height and inclination, as support for understanding the plot of the mass margin. The data range chosen for the analysis considers the possibility to have a parking orbit above the target.

It is evident how the delivered mass by the launch vehicle influences the mass margin. By increasing the height, the delivered mass decreases, with an overall reduction of the mass margin.

By fixing a generic curve of mass margin, it is possible to notice that for inclinations around to 98° there is a peak towards higher altitudes. This value of inclination is close to the inclination of target orbits, making the rendezvous a coplanar manoeuvre and saving a significant quantity of propellant mass. By avoiding the plane change, an expansive manoeuvre in terms of propellant mass, it is possible to obtain a higher mass margin performing the rendezvous from the same height of the parking orbit. By increasing the difference of inclination between the orbits the plane change requires a higher quantity of propellant penalizing the mass margin.

Another evident phenomena is the concentration of curves corresponding to the height of 500 km and inclination of 97°. To explain this concentration it is useful the RPR plot. In this region there is a relative precession rate close to zero (Sun-synchronous orbits). It means that the alignment of the line of nodes

takes a long time, and consequently the quantity of propellant mass required for the atmospheric drag cancellation will be extremely high.

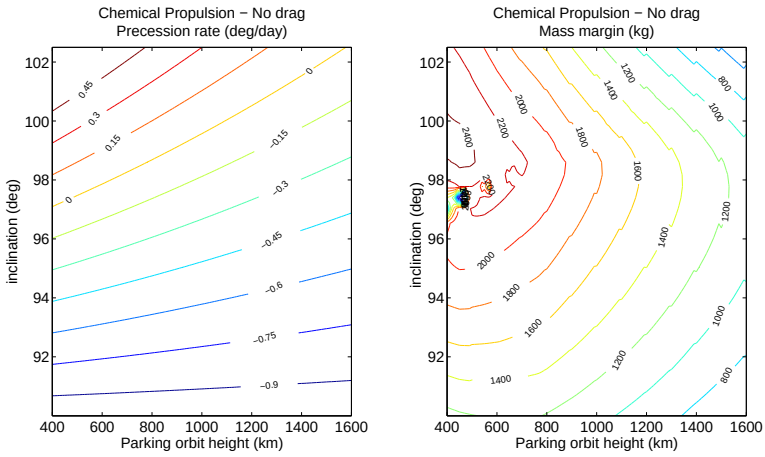

Figure 7.1: RPR ($deg \cdot day^{-1}$) and Mass Margin (kg) as a function of height and inclination of the parking orbit - Chemical Propulsion

It is possible to infer that orbits with low heights (around 400 km) and coplanar to the target (around 98°) are preferred to have a higher mass margin.

7.1.1 Relative Precession Rate and Mass Margin with Atmospheric Drag Effect

For understanding the atmospheric drag effects, an analysis is conducted by fixing height and inclination of the parking orbit for removing the first target ($r_{do} = 772.77\,km$ & $i_{do} = 98.6278°$; $r_{po} = 300\,km$ & $i_{po} = 98.4°$).

Analysis	$m_{p,re}(kg)$	$m_{p,podo}(kg)$	$m_{p,J2}(kg)$	$m_{tot}(kg)$
Without atmospheric drag	135.3809	53.8427	7.1443	196.3680
With atmospheric drag	133.5757	54.7608	7.1443	195.4808

Table 7.1: Propellant mass for de-orbit the first target

By selecting the first target, it is possible to see that the atmospheric drag leads a small amount of propellant mass to be saved. Although during the Hohmann transfer it needs more propellant, in the re-entry phase the drag helps the spacecraft in reducing its velocity, with an overall saving of propellant mass. This is true since the drag effects are more significant in the lower part of the atmosphere and for $h > 480\,km$ the propellant mass for the drag cancellation in negligible.

Mass margin and relative precession rate as function of altitude and inclination are represented in figure 7.2.

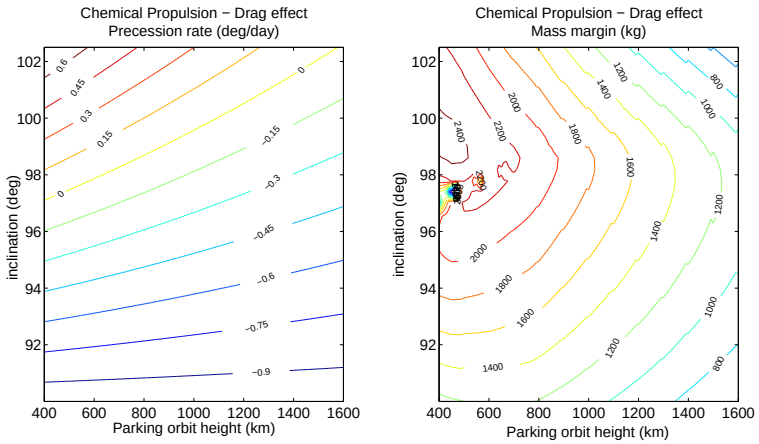

Figure 7.2: RPR ($deg \cdot day^{-1}$) and Mass Margin (kg) as a function of height and inclination of the parking orbit - Chemical Propulsion & Atmospheric Drag

The trend of the mass margin in the analysis considering atmospheric drag effects in Hohmann transfer and re-entry is similar to the previous one. In the comparison between the two models the small amount of propellant mass saved is translated in an increase of the mass margin and the curves move slightly towards higher altitudes.

7.2 Qualitative Identification of the Parking Orbit with Electric Propulsion

The analysis is carried out by considering the target orbit always above to the parking orbit. Thus, in case of failure of the mission the atmospheric drag will re-entry quickly the spacecraft from the parking orbit.

With the aim to identify qualitatively the parking orbit for the removal of five targets from LEO using spacecraft / chaser electrically propelled, the mass margin as a function of height and inclination of the parking orbit is represented in figure 7.3.

The delivered mass by the launch vehicle influences the mass margin, since it decreases as the altitude is higher. For altitudes lower than 400 km there is an asymmetric behaviour due to the initial RAAN of the parking orbit chosen that is lower than the initial RAAN of the target orbit. When the relative precession rate is negative, the angle that has to be swept is the explementary of the difference between the two initial RAANs. Since this difference is about 10-20°, the waiting time on the parking orbit is really long, the propellant mass for the

drag cancellation really high and the mass margin is penalised. This asymmetry is not evident for chemical propulsion since, to focus the attention where the mass margin is higher, in the analysis for electric propulsion the altitude range was shifted starting from lower altitudes (from 200 km) where the atmospheric drag effect is more significant.

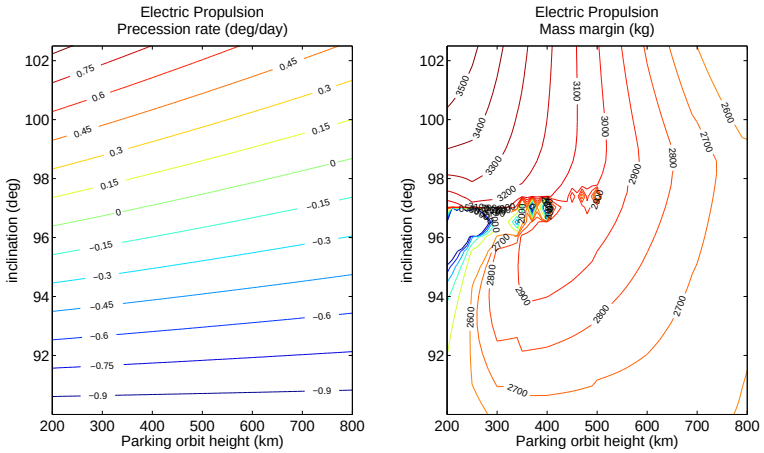

Figure 7.3: RPR ($deg \cdot day^{-1}$) and Mass Margin (kg) as a function of height and inclination of the parking orbit - Electric propulsion

7.2.1 Results for Sensitivity Test

Results and discussion about the sensitivity tests on dry mass, specific impulse and initial RAAN are presented as follow.

7.2.1.1 Sensitivity Test on Dry Mass

The dry mass of the electric spacecraft is reduced by 20%. The effect of this reduction has consequences on the mass margin, as shown in figure 7.4.

The mass margin increases significantly, with higher values in reference to the results obtained with chemical propulsion. In a successive and detailed design, it is necessary to estimate more precisely the mass budget and reduce the dry mass of the spacecraft, that is always one of the most challenging tasks.

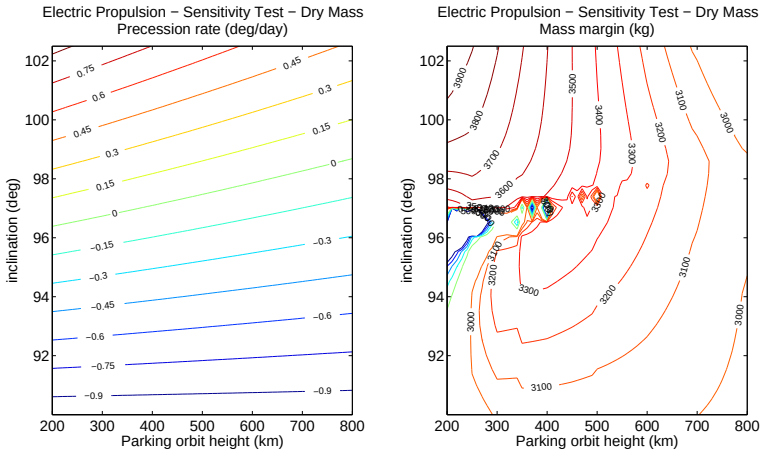

Figura 7.4: RPR ($deg \cdot day^{-1}$) and Mass Margin (kg) as a function of height and inclination of the parking orbit - Sensitivity test on dry mass

7.2.1.2 Sensitivity Test on Specific Impulse

The mass margin as a function of altitude and inclination of the parking orbit for a removal mission of five targets is represented in figure 7.5.

The propellant mass saved during the manoeuvres because of the high performance engine compensates the increasing dry mass of the spacecraft. In this way, the mass margin is greater than the case with a low performance engine. Obviously, the conclusion is valid considering reliable the values obtained with the model for dry mass estimation.

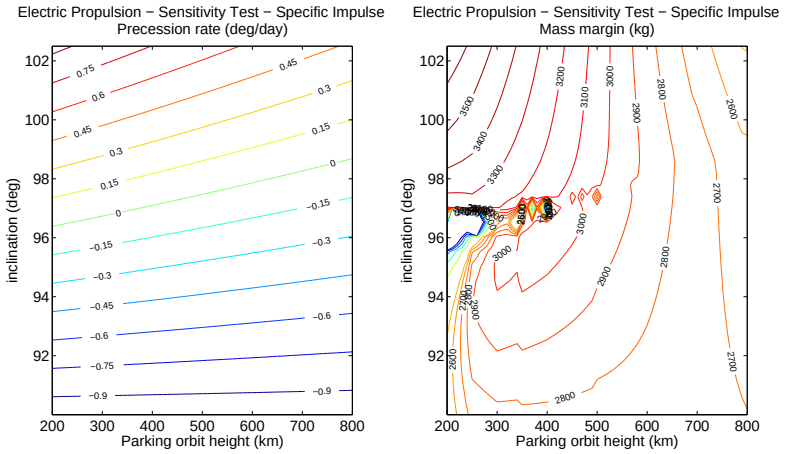

Figure 7.5: RPR ($deg \cdot day^{-1}$) and Mass Margin (kg) as a function of height and inclination of the parking orbit - Sensitivity test on specific impulse

7.2.1.3 Sensitivity Test on Initial RAAN

The first test conducted with initial RAAN for each chaser equal to:

$$\Omega_{in,s/c} = \Omega_{in,T} - 20^\circ \tag{7.1}$$

produces effects on the mass margin as reported in figure 7.6.

The solution does not introduce significant changes and it is not viable because each spacecraft should lift off from the Earth in different times, since the initial RAAN is determined during the launch.

In the second test, for each spacecraft chaser has been chosen:

$$\begin{aligned} \Omega_{in,s/c} &= \Omega_{in,T} - 20^\circ \quad \dot{\Omega}_{po} - \dot{\Omega}_{to} > 0 \\ \Omega_{in,s/c} &= \Omega_{in,T} + 20^\circ \quad \dot{\Omega}_{po} - \dot{\Omega}_{to} < 0 \end{aligned} \tag{7.2}$$

Results are presented in figure 7.7.

The symmetry is restored but particular benefits are not registered on the mass margin. For this reason, the analysis is not relevant for further development of the project.

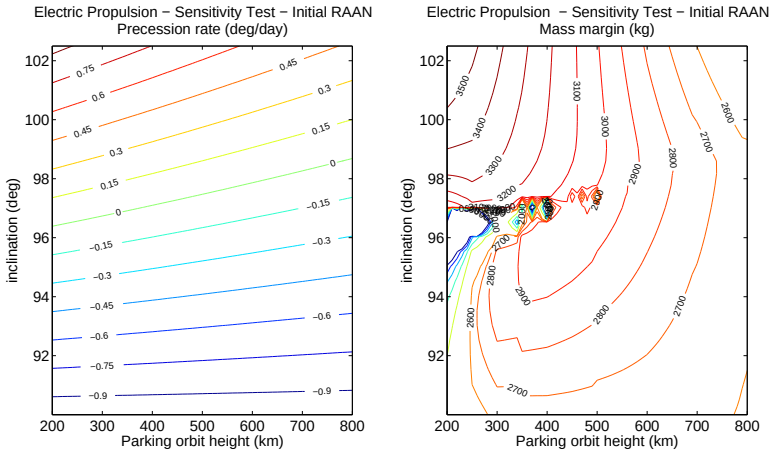

Figure 7.6: RPR ($deg \cdot day^{-1}$) and Mass Margin (kg) as a function of height and inclination of the parking orbit - Sensitivity test on initial RAAN

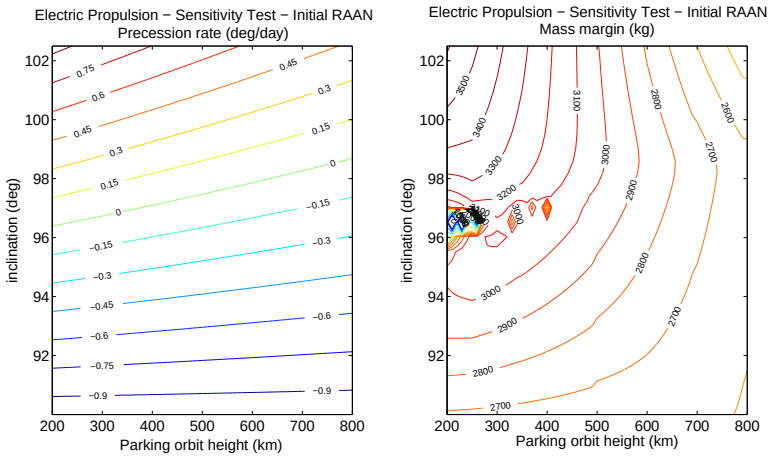

Figure 7.7: RPR ($deg \cdot day^{-1}$) and Mass Margin (kg) as a function of height and inclination of the parking orbit - Sensitivity test on initial RAAN

7.3 Qualitative Identification of the Parking Orbit with Hybrid Propulsion

The presentation and discussion of results for hybrid propulsion systems is differentiated for the three concepts of mission: hybrid spacecraft, hybrid system and hybrid system with orbiting bus.

7.3.1 Hybrid Spacecraft

By considering the atmospheric drag and gravitational perturbation effects for each target, the spacecraft/chaser using electric propulsion system compensates the atmospheric drag during the waiting time in the parking orbit for the alignment of the line of nodes, performs a rendezvous with the debris and a plane change e de-orbits it in the parking orbit. The final burn for the re-entry in atmosphere is demanded to chemical propulsion system.

As shown in the previous sections, since by lowering the altitude of the parking orbit it is possible to obtain higher values of mass margin, this altitude is always above the target orbit.

7.3.1.1 Qualitative Identification of the Parking Orbit with Hybrid Spacecraft

With the aim to identify qualitatively the best parking orbit in the removal mission of five debris from LEO, using spacecraft with hybrid propulsion systems, the relative precession rate and the mass margin are presented in figure 7.8.

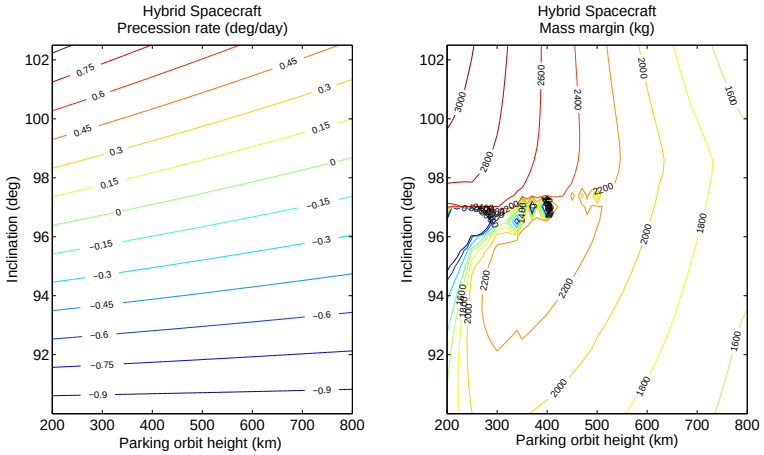

Figure 7.8: RPR ($deg \cdot day^{-1}$) and Mass Margin (kg) as a function of height and inclination of the parking orbit - Hybrid spacecraft

By demanding the final burn to the chemical propulsion system, the hybrid spacecraft ensures a reliability rather than the purely electric propulsion system about the possibility to provide a more accurate estimation about the re-entry point in atmosphere. Also, the mass margin is lower than the one obtained with electric propulsion and higher than the chemical one. For low altitude orbit and high inclination the maximum mass margin is around 3000 kg.

Although there is an improvement in the control of the re-entry point, the chemical propulsion system penalises the mass margin when the altitude increases, because the re-entry from an high parking orbit requires a significant

quantity of propellant mass. In this range of altitude the mass margin is lower than the mass margin obtained with electric propulsion.

As obtained with the electric propulsion system, a relative precession rate close to zero or negative leads to have extremely long waiting times for the alignment of the line of nodes. At low altitude and inclination, where the atmospheric drag effect is significant, the quantity of propellant mass and the duration of the mission become prohibitive in the achievement of the aim of the study.

It is important to define precisely the spacecraft in all its systems and subsystems for estimating the dry mass. If the attention is focused on minimising the mass, the results obtained encourage the use of hybrid spacecrafts.

7.3.2 Hybrid System with Single Debris Recovery - Re-entry from DO

After the atmospheric drag compensation on the parking orbit, the electric shuttle has the task to perform the rendezvous with the debris carrying all the chemically propelled tugs for the re-entry. The target is docked and grappled by the robotic arm and the chemical tug realises the final disposal in atmosphere. The shuttle comes back to the parking orbit and it performs the same manoeuvres for collecting the other targets.

Important consideration is about the rendezvous and the manoeuvre for bringing the shuttle back to the parking orbit. Due to the gravitational perturbation effect (J_2), the RAANs of the parking orbit and target orbit for the $i-th$ debris are shifted respect the initial value as follow:

$$\Omega^{'}_{in,doi} = \Omega_{in,doi} + \dot{\Omega}_{do,i} \sum_{j=1}^{i-1} t_{miss,Dj} \tag{7.3}$$

$$\Omega^{'}_{in,po} = \Omega_{in,po} + \dot{\Omega}_{po} \sum_{j=1}^{i-1} t_{miss,Dj} \tag{7.4}$$

where it is necessary to know the durations of all the previous manoeuvres respect to the $i-th$ debris. Since the shuttle has to carry the propellant mass for the whole mission, it is necessary to know the propellant mass for the successive manoeuvres respect the i-th debris.

The code documentation for the disposal of a generic debris is presented in scheme A in figure 7.9.

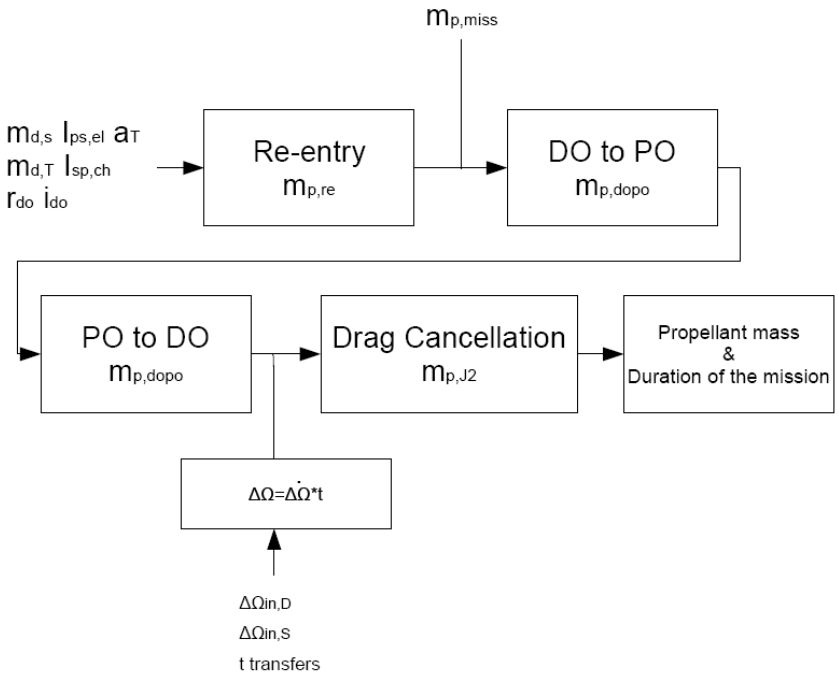

Figure 7.9: Code documentation - Scheme A

The removal operations are dependent one from each other and the target are sorted by altitude following a decreasing criteria. The code produces results depending on the manoeuvres and the debris removal order. Since initially there are no information about the propellant mass and duration of the mission, it is necessary to create first try values for $m_{p,miss}$ and t_{miss}. Using the scheme A for the fifth debris as independent from the others, it is possible to generate a first value for $m_{p,miss}$. After this, using the same scheme on the same target, a generic value for the duration of the mission is generated (t_{miss}).

The stopping criteria is satisfied when the duration of the mission differs of less than one day between two following iterations:

$$\left| t_{miss}^{(k)} - t_{miss}^{(k-1)} \right| < 1\, day \tag{7.5}$$

The final code architecture is presented in figure 7.10.

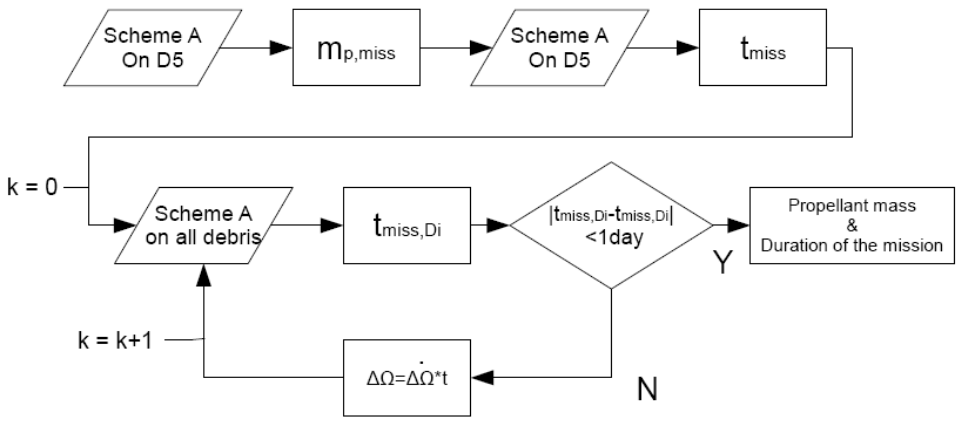

Figure 7.10: Code documentation - Hybrid system

7.3.2.1 Qualitative Identification of the Parking Orbit with Hybrid System

The qualitative optimization of the parking orbit is presented in figure 7.11.

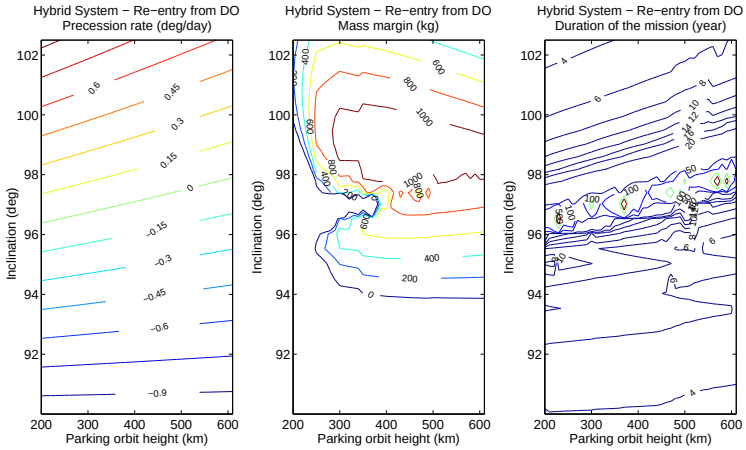

Figure 7.11: RPR ($deg \cdot day^{-1}$) and Mass Margin (kg) as a function of height and inclination of the parking orbit - Hybrid system

The maximum mass margin is lower than the one obtained with chemical propulsion. Despite high inclination are still preferred, this proposal encourages the use of orbits with high altitude. Since the waiting time in the parking orbit is now a preponderant event in terms of duration of the mission, and then in terms of propellant mass for the drag cancellation, the best solution is related

to low density orbits.

The duration of the whole mission is the real limit of the solution. Orbits with high altitude have a small relative precession rate, then the waiting time for the alignment of line of nodes is really long. By selecting the curve of mass margin equal to 1000 kg, it is possible to see that the durations are included between 6 and 500 years.

Mission duration higher than ten years are not acceptable, since the operative life of the spacecraft is limited by the degradation of materials, reducing the performance of the spacecraft and the failure of the mission.

7.3.3 Hybrid System with Bus and Single Tug

The bus is on the parking orbit carrying the chemically propelled tug, that performs the re-entry once the shuttle collects all the debris, and the propellant mass necessary for each shuttle operation. After the disposal of each target to the parking orbit, the shuttle docks the debris to the bus and refuels it for removing the next debris.

The manoeuvres are dependent one each other in terms of duration of the operations, but independent about the propellant mass. For this reason, the code does not require an iterative cycle as for the hybrid system.

The RAAN adjustment manoeuvre is expensive in terms of propellant mass and for this reasons it is not considered. To perform the rendezvous between the shuttle and the bus after collecting one target, it is necessary to wait for the alignment of line of nodes between target and parking orbit. A drag cancellation manoeuvre is performed to synchronise shuttle and bus.

The code documentation for the removal of a generic debris in presented in scheme B in figure 7.12.

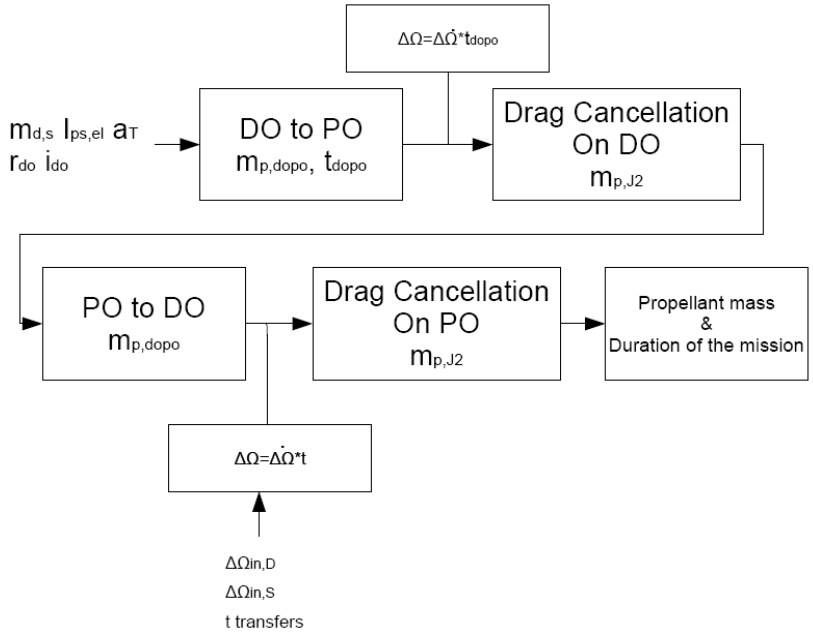

Figure 7.12: Code documentation - Scheme B

By underlining the independency of the re-entry respect to the manoeuvres of the shuttle, the final architecture of the code is represented in figure 7.13.

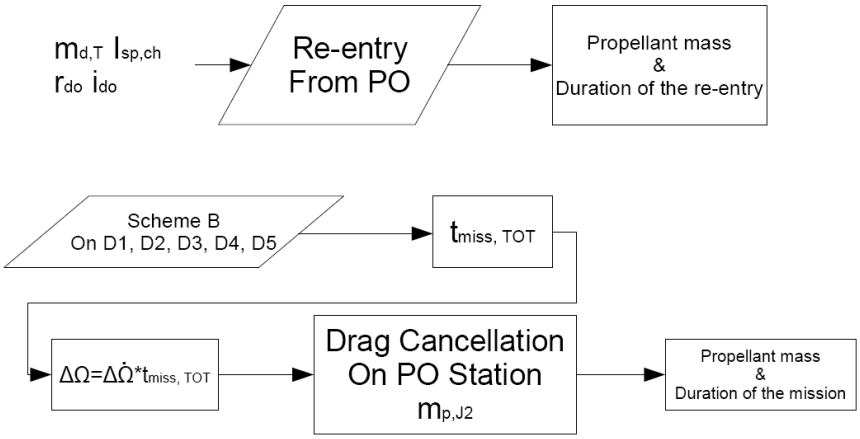

Figure 7.13: Code documentation - Hybrid system with bus

7.3.3.1 Qualitative Identification of the Parking Orbit with Hybrid System and Bus

Relative precession rate, mass margin and duration of the mission as functions of height and inclination of the parking orbit are reported in figure 7.14.

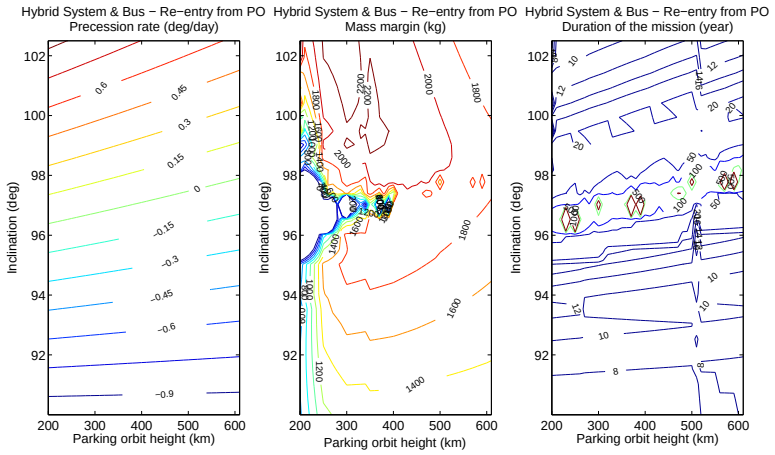

Figure 7.14: RPR ($deg \cdot day^{-1}$) and Mass Margin (kg) as a function of height and inclination of the parking orbit - Hybrid system with bus

In terms of mass margin, the maximum value is 2200 kg with durations of the mission between ten and twenty years. Also in this case low inclinations are preferred for a higher mass margin, which benefits for the reduced weight of the spacecraft that the launcher has to deliver in orbit. Since the waiting times during the alignments are significant, the benefits of low density orbits and high delivered mass by launcher vehicle are balanced for altitudes between 300 and 400 km.

Assuming the validity of the model for spacecraft dry mass estimation, this solution has the most interesting potential for this preliminary study.

7.4 Comparisons

The task of the study is to quantify the fuel used for electric and chemical propulsion systems and find the most efficient architecture. By considering the same transfer, therefore with the aim of removing the same target, and parking orbit, it has been made a comparison between chemical and electric prolusion focusing the attention on propellant mass and duration of each manoeuvre.

System	$m_{p,re}(kg)$	$t_{re}(day)$	$m_{p,po2to}(kg)$	$t_{po2to}(day)$	$m_{p,J2}(kg)$	$t_{w,po}(day)$
Chemical	134.5757	0.0322	76.3393	0.0311	4.9893	34.4859
Electric	41.7626	5.7685	8.4118	5.3565	0.9591	34.8710

Table 7.2: Comparison between Chemical and Electric Propulsion Systems

Propulsion System	$m_{p,tot}(kg)$	$t_{tot}(day)$
Chemical	215.9043	34.5512
Electric	51.1335	45.9960

Table 7.3: Total propellant mass and duration of the mission

The duration of the mission is increased of 10 days and the propellant mass saved is about 165 kg.

In terms of propellant mass the electric propulsion system is a better solution respect to the chemical propulsion system and the dry mass of the electric spacecraft is pretty much the same of the chemical one. By observing the mass margin, there are advantages in using an electric propulsion system since the maximum mass margin is 3500 kg against 2400 kg obtained with the chemical propulsion.

With the aim to underline strengths and weaknesses of the hybrid spacecraft, a comparison with the purely electrically propelled spacecraft is made choosing the debris orbit with the following parameters: $r_{do} = 772.77\,km, i_{do} = 98.6278°\Omega_{d,in} = 135.0506°$.

Three different parking orbits are analyzed with the intent to observe the effects of high or low heights and inclinations.

- Parking orbit: $r_{po} = 210\,km$, $i_{po} = 102.5°$ & $\Omega_{in,po} = 120°$

System	$m_{p,re}(kg)$	$m_{p,podo}(kg)$	$m_{p,J2}(kg)$	$m_{p,tot}(kg)$
Electric	41.7626	23.2162	2.4408	67.4197
Hybrid S/C	31.6419	28.1448	1.2034	70.8580

Table 7.5: Comparison between electric and hybrid spacecrafts (a) - Propellant mass

System	$t_{re}(day)$	$t_{podo}(day)$	$t_{w,po}(day)$	$t_{tot}(day)$
Electric	5.7685	13.3935	7.9452	27.1072
Hybrid S/C	0.0302	13.2962	3.9143	22.5974

Table 7.7: Comparison between electric and hybrid spacecrafts (a) - Duration of the transfers

- Parking orbit: $r_{po} = 300\,km$, $i_{po} = 102.5°$ & $\Omega_{in,po} = 120°$

System	$m_{p,re}(kg)$	$m_{p,podo}(kg)$	$m_{p,J2}(kg)$	$m_{p,tot}(kg)$
Electric	41.7626	22.6098	0.2721	64.6446
Hybrid S/C	49.6585	28.3112	0.0905	86.5059

Table 7.9: Comparison between electric and hybrid spacecrafts (b) - Propellant mass

System	$t_{re}(day)$	$t_{podo}(day)$	$t_{w,po}(day)$	$t_{tot}(day)$
Electric	5.7685	12.4363	9.8940	28.0989
Hybrid S/C	0.0305	12.4351	3.2898	20.1815

Table 7.11: Comparison between electric and hybrid spacecrafts (b) - Duration of the transfers

- Parking orbit: $r_{po} = 500\,km$, $i_{po} = 102.5°$ & $\Omega_{in,po} = 120°$

System	$m_{p,re}(kg)$	$m_{p,podo}(kg)$	$m_{p,J2}(kg)$	$m_{p,tot}(kg)$
Electric	41.7626	21.6946	0.0099	63.4672
Hybrid S/C	88.7150	28.9941	0.0013	122.8303

Table 7.13: Comparison between electric and hybrid spacecrafts (c) - Propellant mass

System	$t_{re}(day)$	$t_{podo}(day)$	$t_{w,po}(day)$	$t_{tot}(day)$
Electric	5.7685	10.7598	14.8925	31.4208
Hybrid S/C	0.0312	10.7615	1.9245	15.2127

Table 7.15: Comparison between electric and hybrid spacecrafts (c) - Duration of the transfers

When the height of the parking orbit increases, the re-entry with chemical propulsion system is more penalising. The duration of the transfers decreases because the re-entry with chemical propulsion is quicker, but the total propellant mass is reduced only for low altitudes and high inclinations. Globally, there is an advantage for the mass margin since the increasing dry mass is compensated by the propellant mass saved for using a high specific impulse engine.

7.5 Extra-Target Removable

The core of the analysis is to provide a methodology for identifying the best parking orbit when a specific propulsion system is used. The qualitative optimization of the parking orbit is based on the study of the mass margin.

The aim of the study is to make a trade-off between conventional chemical and electric propulsion systems using the mass margin, that is an indicator of the extra-mass deliverable by the launcher and therefore it includes the dry mass of the spacecraft. For this reason, the mass margin is strictly related to the propulsion system examined and the results obtained can not be directly compared.

It is important to estimate a reference value for each propulsion system proposed, as the total mass necessary to remove a generic target. By comparing this value with the mass margin is possible to understand how many extra-targets can be removed with the same mission or launch.

The reference value for the removal of a target includes the dry mass of the spacecraft and the total propellant mass necessary for the disposal manoeuvres. Whilst the dry mass of the spacecraft is considered constant, a generic value of total propellant mass for the mission operations has to be generated. Selected the propulsion system and by averaging the total propellant mass values related to a positive mass margin, it is possible to obtain a mean value useful for this purpose.

The values of interest for this analysis, considering the number of extra-target removable are presented in table 7.16.

Propulsion System	$m_d(kg)$	$\overline{m_p}\,(kg)$	$MM\,(kg)$	Extra-Target
Chemical	389.5	177.2	2400	+4
Electric	382.3	63.2	3500	+7
Electric - ST on m_d	305.8	61.7	3900	+10
Electric - ST on I_{sp}	404.5	32.4	3600	+8
Hybrid Spacecraft	462.4	69.2	3000	+5
Hybrid System	$790 + 455 \cdot 5$	2500/5	1000	+1[1]
Hybrid System and Bus	820+755+980	1500/5	2200	+5[2]

Table 7.16: Extra-Target removable

It is important to notice that for hybrid system and hybrid system with bus solutions, it should be necessary a deeper analysis to understand how the spacecraft changes if it has to deliver more targets. However, as preliminary analysis this is acceptable.

7.6 Wider Issues

The mission architecture proposed is not the only one that can be conceived. Depending on the target and aims, different active debris removal mission can

be realised. This is a suitable architecture for removing large targets orbiting in LEO, focusing the attention on the possibility to consider different propulsion systems. The active removal missions illustrated are characterized by the presence of perturbation effects as atmospheric drag and Earth's oblateness.

The main assumptions and simplifications adopted in the model regarding spacecrafts and manoeuvres are:

- In electric propulsion system, since the total mass of the spacecraft varies slightly during the mission and thrust is constant, it is possible to consider the acceleration thrust constant, as well. This assumption is useful for the implementation of the code in the mass margin estimation.
- Important issue is about the mass of the tanks. Depending on the propellant mass that the tank carries its mass varies. An iterative process about the dry mass of the spacecraft as input data would be necessary. Actually, the mass of tanks variation due the propellant mass is just few decimal percent and it allows to avoid the implementation of an iterative process and raise the computational cost.
- A model for spacecraft mass estimation has been necessary during the study for creating reliable input data for the analysis of the active debris removal missions. Although there are data about characteristics of generic subsystems and empiric relations for their mass estimation, the validation of the model is complex for the specificity of each spacecraft. Therefore, it is important to consider a certain margin of uncertainty.
- An additional propellant mass should be quantified because no station keeping manoeuvres are considered in the mission architecture.

About the code for mass margin estimation it is important to underline that even if high-accuracy methods for the integration of equations of motion are used, genetic algorithms for mass margin optimisation have not been implemented. This is a preliminary study and a qualitative identification of the best parking orbit, in terms of altitude and inclination, is considered acceptable.

Chapter 8

Conclusions

Debris proliferation in space environment is an impending problem for preserving future missions.

Although prevention measures (IADC guidelines, NASA Handbook for Limiting Orbital Debris) with the intent to regulate and limit the space traffic are adopted, the necessity of reducing the increasing quantity of space debris leads to conceive and test the effectiveness of active debris removal missions (ADR). ADR missions are devised for controlling the effective number of large objects, as launch vehicle orbital stages or derelict spacecraft which no longer serve a useful purpose, orbiting in densely populated and with commercial interests regions (Sun-Synchronous Orbit, SSO).

With the aim to select the most efficient mission design, the analysis is carried out developing codes for the estimation of extra-targets removable respect to the ones scheduled initially, using conventional chemical and electric propulsions systems.

There is an increase of the mass margin and the possibility of launching a higher number of electrically propelled spacecraft respect to the mission conceived with chemically propelled spacecraft.

Therefore, the preliminary project shows that electric propulsion is preferred over purely chemical propulsion. Mission architecture with electrically propelled spacecraft gives a higher mass margin and the possibility to remove seven extra-targets.

A high number of targets can be removed annually; this encourages the use of ADR mission for space debris proliferation control in LEO.

The difficulties in controlling the re-entry point into the atmosphere reduces the feasibility of using electrically propelled spacecraft for active debris removal missions. In order to make re-entry into the atmosphere more reliable, it is necessary to integrate chemical propulsion units.

About the hybrid proposals, the hybrid spacecraft introduces benefits in terms of mass margin, giving the possibility to remove five extra-target. Hybrid systems are interesting solutions since potentially they can remove more targets, but these options have problems related to the duration of the missions making

them unfeasible.

In terms of qualitative identification of the parking orbit for maximising the mass margin, altitudes around 400 km and inclination close to 98° are chosen. In this way, waiting time on the parking orbit for the alignment of line of nodes is minimised and atmospheric drag effects are not too penalising. The transfer to perform the rendez-vous between the spacecraft and debris is coplanar and the propellant mass for the plane change is saved. Except for the hybrid system where the waiting time in the parking orbit is extremely long, the altitudes chosen are higher for the lower values of density.

8.1 Further Work

Further work can be based on the development of more effective mission architectures. Recent studies present active removal missions using a "Thruster De-orbiting Kit" (TDK) for the re-entry of the target [6]. This unit is really light (30 kg, $I_{sp} = 288\,s$) and can deliver large debris as Ariane IV upper stages. A second iteration in the design phase could consider the use of these thrusters.

The results obtained encourage the use of hybrid systems and the model for spacecraft dry mass estimation should be improved. The importance of being confident with input data is fundamental for the validity of the analysis.

Greater attention should be given to the identification of the parking orbit for optimising the mass margin. Genetic algorithms can be used with the aim to optimise the number of target removable with a single launch.

Appendix A

Model for Spacecraft Dry Mass Estimation

Spacecraft dry mass estimation is one of the most challenging tasks during the preliminary design. It is difficult to provide accurate values about dry mass, but empiric relations based on the knowledge of existing spacecraft and propulsion systems lead to the possibility to obtain realistic and reliable estimations.

The interest in a model for spacecraft dry mass estimation is about the possibility to create reliable values as input data for the code during the analysis of different strategies and scenarios for space debris removal missions. By conceiving different kinds of mission architecture there is the necessity to estimate dry mass of an electrically propelled spacecraft with a high performance engine and different hybrid systems (chemical and electric systems combined).

The validation of the model is complex for the specificity of each spacecraft considered in the study. Although there are data about characteristics of generic subsystems and empiric relations for their mass estimation, it is necessary to reserve a certain margin of uncertainty.

A.1 Electrically Propelled and High Performance Spacecraft

With the intent to overlook the effects of using a propulsion system with high performance, during the sensitivity test an electric engine with high specific impulse is used.

It may introduce benefits on mass margin, since a significant quantity of propellant mass can be saved to perform the removal manoeuvres. On the other hand, a high specific impulse engine requires higher electric power and a power system more complex and heavy. The increasing dry mass of the spacecraft is in contrast with the saving of propellant mass, decreasing the mass margin.

For this reason, dry mass estimation consists in subtracting engine and power

systems masses from the total mass of the known spacecraft, and replacing them with the parameters of the high performance system. By distinguishing low performance (LP) and high performance (HP) spacecraft:

$$m_{d,HP} = m_{d,LP} - m_{engine,LP} - m_{pow-sys,LP} + m_{engine,HP} + m_{pow-sys,HP} \quad \text{(A.1)}$$

It is important to define engine and power system. The engine is considered as thrusters (T) and propellant feeding system (PFS) and the power system as power control unit (PCU) and solar array (A):

$$m_{engine} = m_{thruster} + m_{PFS} \quad \text{(A.2)}$$

$$m_{pow-sys} = m_{PCU} + m_{array} \quad \text{(A.3)}$$

The mass of the subsystems is strongly dependent on the selected technology. The main technologies about electric engines are reported as follow:

	PPT	SPT	Ion Thruster	FEEP
Propellant	Teflon	Xe	Xe	Caesium
$P_R(kW)$	0.001 - 0.025	0.15 - 1.5	0.4 - 2.0	0.00001 - 0.12
$T(mN)$	0.01 - 1	40 - 200	15 - 200	0.001 - 5
$I_{sp}(s)$	300 - 1000	1500 - 1700	1800 - 3500	5000 - 10000

Table A.1: Electric engines technologies

where: PPT is Pulsed Plasma Thruster, SPT is Stationary Plasma Thruster and FEEP is Field Emission Electric Propulsion. The requested input power is P_R.

The choice is on an ion thruster engine (NSTAR, NASA's Ion thruster), and knowing the characteristics of DR LEO spacecraft (low performance), the table A.2 makes a comparison between the two engine.

	DR LEO	NSTAR
$P_R(kW)$	1.2	2.3
$I_{sp}(s)$	1640	3300
$T\,(mN)$	68	92
$m_{thruster}(kg)$	29	8

Table A.2: LP vs HP - Engines

Reasonably considering the propellant feeding system mass equal to 9 kg for both the engines, the empiric relations for power control unit and array masses [20, 21] are:

$$m_{PCU} = 0.0049 \cdot P_R + 2.0987 \quad \text{(A.4)}$$

$$m_{array} = 0.04 \cdot P_R \tag{A.5}$$

Table A.3 presents the values used for high performance spacecraft dry mass estimation.

	DR LEO	NSTAR
$m_{thruster}(kg)$	29	8
$m_{PFS}(kg)$	9	9
$m_{PCU}(kg)$	9.5	13.5
$m_{array}(kg)$	60	92
$m_d(kg)$	389.5	404.5

Table A.3: LP vs HP - Dry mass estimation

Spacecraft dry mass increased of 15 kg. As shown, the saving of propellant mass due the high performance engine compensates the increasing of the dry mass, with an overall increment of the mass margin.

A.2 Hybrid Spacecraft and Systems

The proposal is to conceive hybrid spacecraft that, combining chemical and electric propulsion, uses the most affordable system depending on the specific manoeuvre.

The qualitative analysis for the identification of the parking orbit requires values of spacecraft dry mass as input data. Respect with the mission architecture proposed, spacecraft have to fulfil different tasks and have particular characteristics. In this section, a simple and straightforward method for dry mass estimation is proposed, with the peculiarity of estimating the dry mass depending on the tasks of the spacecraft, then on the payload [21].

In this mission the payloads are robotic arms used for grappling and docking the target or for transporting and releasing chemical tugs (dispenser). Thus, the spacecraft dry mass is:

$$dry\,mass = 4.8 \cdot Payload\,mass \tag{A.6}$$

It is necessary to estimate the payload mass for each spacecraft configuration. For this reason, it is used a simple proportion with reference to the robotic arm on the ISS, the Canadarm, where values of dry and retrieved mass are known. Chosen the retrieved mass by the generic robotic arm, its dry mass is:

$$m_{d,arm} = \frac{m_{d,CA} \cdot m_{r,arm}}{m_{r,CA}} \tag{A.7}$$

where $m_{d,CA} = 450\,kg$ and $m_{r,CA} = 32.5\,ton$ [22].

Since the mass of the debris / target is 1.6 tons, the robotic arms for one or five targets wheight respectively 23 and 165 kg. About the dispenser, since

the total mass of a tug (considering dry mass and propellant mass for a generic re-entry from low earth orbit) is approximately 800 kg, the dispenser dry mass for five tugs is 85 kg.

An import clarification is about the re-entry for the chemical tug. If the re-entry is performed from the debris or parking orbit, the mass of the propulsion system is different and as a function of the propellant mass necessary [21] following the relation:

$$Kick\ stage\ mass = 1.2 \cdot Propellant\ mass \tag{A.8}$$

and since:

$$Propulsion\ system\ mass = 10\%\ Dry\ mass \tag{A.9}$$

the mass of a generic tug is:

$$Dry\,mass = 4.8 * Payload\,mass - Propulsion\,system\,mass + Kick\,stage\,massa \tag{A.10}$$

The following tables present the payload types and their mass in each spacecraft configuration. The dry mass of the spacecraft for the corresponding mission architecture is:

	Payload	$m\ (kg)$
Electric Shuttle	Robotic arm for 1 debris	60
	Robotic arm for 5 debris	165
	Dispenser	85
	Antenna	4
Chemical Tug	Robotic arm for 1 debris	60
	Robotic arm for 5 debris	165
	Antenna	4
Electric Bus	Dispenser	85
	Propellant Feeding System	100
	Antenna	4

Tabella A.4: Payload definition for spacecraft configurations

	Mission Architecture		$m_d(kg)$
Electric Shuttle	Deliver 5 tugs	Single recovery	790
		Cascade recovery	1200
Chemical Tug	De-orbit 1 target	Re-entry from PO	365
		Re-entry from DO	455
	De-orbti 5 targets	Re-entry from PO	755
		Re-entry from DO	840
Electric Bus	Bus sulla PO		980

Tabella A.5: Dry masses for different mission architecture

The validity of the model for mass estimation gives the possibility to be confident with the obtained results. Also in this case, for the specificity of each spacecraft it is not possible to compare these values with existing ones and it is necessary to keep a margin of uncertainties about the estimations and results.

Bibliography

[1] D. Baiocchi, W. Welser (2010). 'Confronting Space Debris'. National Defense Research Institute. RAND Corpoation.

[2] N. L. Johnson (2007). 'Debris Removal: An Opportunity for Cooperative Research?'. NASA Johnson Space Center Improving our Vision II: Building Transparency and Cooperation 25-26 October 2007 INMARSAT Headquarters, London.

[3] F. Alby (2005). 'Spot 1 End of Life Disposition Manoeuvres'. Advances in Space Research 35 (2005) 1335–1342.

[4] L. Anselmo, C. Pardini (2008). 'Space Debris Mitigation in Geosynchronous Orbit'. Advances in Space Research 41 (2008) 1091–1099.

[5] L. Nicholas, E. G. Johnson, Stansbery (2010). 'The New NASA Orbital Debris Mitigation Procedural Requirements and Standards'. Acta Astronautica 66 (2010) 362 – 367.

[6] M. M. Castronuovo (2011). 'Active Space Debris Removal - A Preliminary Mission Analysis and Design'. Acta Astronautica, Vol. 69, pag. 848-859.

[7] Data are from file catalog_31_2010_06_23_pm website Spacetrack.org

[8] N. L. Johnsons, C. Liou (2010). 'A Parametric Study on Using Active Debris Removal for LEO Environment Remediation'. NASA Johnson Space Center, Houston, USA.

[9] V. A. Chobotov (2002). 'Orbital Mechanics'. American Institute of Aeronautics and Astronautics.

[10] W. H. Press (2007). 'Numerical Recipes : The Art of Scientific Computing'. Third Edition, Cambridge University Press.

[11] S. J. Isakowitz, J.B. Hopkins and J.P. Hopkins (2004). 'International Reference Guide to Space Launch Systems'. AIAA, Reston, VA, USA.

[12] Perez E. (2006). 'Soyuz from the Guiana Space Centre'. User's Manual. Tech. rep. Arianespace.

[13] S. Hobbs (2010). 'DR LEO: Summary of the Group Design Project', MSc in Astronautics and Space Engineering 2009/10. College of Aeronautics report 1001, Cranfield University.

[14] D. G. King-Hele (1987). 'Satellite Orbits in an Atmosphere : Theory and Applications'. Blackie.

[15] J. E. Pollard (2005). 'Low-Thrust Manoeuvres for LEO and MEO Missions'. AIAA-99-2870, The Aerospace Corporation. Los Angeles.

[16] J. E. Pollard (2005). 'Evaluation of Low-Thrust Orbital Manoeuvres'. AIAA-98-3486, The Aerospace Corporation. Los Angeles.

[17] E. G. C. Burt (1967). 'On Space Manoeuvres with Continuous Thrust'. Planetary Space Science, Vol. 15, pag. 103-122. Pergamon Press, Northern Ireland.

[18] W. C. P. Fernando (2004). 'Feep Thruster Nano-Satellite Applications'. PhD Thesis, Cranfield University.

[19] http://www.grc.nasa.gov/WWW/ion/past/90s/nstar.htm

[20] N. Wallace, C. Saunders (2009). 'The in-orbit performance and status of the GOCE ion propulsion assembly (IPA)'. ESA Publications Division, Noordwjik, The Netherlands.

[21] J. R. Wertz, W. J. Larson (1999). 'Space Mission Analysis and Design '. Third Edition , Kluwer Academic Publishers, Torrance.

[22] http://www.nasa.gov/ mission_pages/ station/ structure/ elements/ subsystems.html